Abiotic Input of Fixed Nitrogen by Bolide Impacts to Gale Crater During the Hesperian: Insights From the Mars Science Laboratory

Rafael Navarro-González[1] (iD), Karina F. Navarro[1] (iD), Patrice Coll[2], Christopher P. McKay[3] (iD), Jennifer C. Stern[4] (iD), Brad Sutter[5] (iD), P. Douglas Archer Jr[5], Arnaud Buch[6], Michel Cabane[7], Pamela G. Conrad[4], Jennifer L. Eigenbrode[4] (iD), Heather B. Franz[4], Caroline Freissinet[7], Daniel P. Glavin[4] (iD), Joanna V. Hogancamp[5] (iD), Amy C. McAdam[4] (iD), Charles A. Malespin[4], F. Javier Martín-Torres[8,9], Douglas W. Ming[10] (iD), Richard V. Morris[10], Benny Prats[11], François Raulin[2], José Antonio Rodríguez-Manfredi[12], Cyril Szopa[7,13] (iD), María-Paz Zorzano-Mier[8,12], Paul R. Mahaffy[4] (iD), Sushil Atreya[14], Melissa G. Trainer[4], and Ashwin R. Vasavada[15] (iD)

[1]Instituto de Ciencias Nucleares, Universidad Nacional Autónoma de México, Mexico City, Mexico, [2]Laboratoire Interuniversitaire des Systèmes Atmosphériques, CNRS UMR 7583, Université Paris-Est Créteil, Université Paris Diderot, Créteil, France, [3]NASA Ames Research Center, Moffett Field, CA, USA, [4]NASA Goddard Space Flight Center, Greenbelt, MD, USA, [5]Jacobs, NASA Johnson Space Center, Houston, TX, USA, [6]Ecole Centrale Paris, Châtenay-Malabry, France, [7]Laboratoire Atmosphère, Milieux, Observations Spatiales, UMR CNRS 8190, Université Versailles Saint-Quentin en Yvelines, UPMC Université Paris 06, Guyancourt, France, [8]Department of Computer Science, Electrical and Space Engineering, Luleå University of Technology, Luleå, Sweden, [9]Instituto Andaluz de Ciencias de la Tierra (CSIC-UGR), Granada, Spain, [10]NASA Johnson Space Center, Houston, TX, USA, [11]NASA/eINFORMe, Inc., Goddard Space Flight Center, Planetary Environments Laboratory, Greenbelt, MD, USA, [12]Centro de Astrobiología (INTA-CSIC), Madrid, Spain, [13]Institut Universitaire de France, Paris, France, [14]Department of Atmospheric, Oceanic and Space Sciences, University of Michigan, Ann Arbor, MI, USA, [15]Jet Propulsion Laboratory, California Institute of Technology, Pasadena, CA, USA

Abstract Molecular hydrogen (H_2) from volcanic emissions is suggested to warm the Martian surface when carbon dioxide (CO_2) levels dropped from the Noachian (4100 to 3700 Myr) to the Hesperian (3700 to 3000 Myr). Its presence is expected to shift the conversion of molecular nitrogen (N_2) into different forms of fixed nitrogen (N). Here we present experimental data and theoretical calculations that investigate the efficiency of nitrogen fixation by bolide impacts in CO_2-N_2 atmospheres with or without H_2. Surprisingly, nitric oxide (NO) was produced more efficiently in 20% H_2 in spite of being a reducing agent and not likely to increase the rate of nitrogen oxidation. Nevertheless, its presence led to a faster cooling of the shock wave raising the freeze-out temperature of NO resulting in an enhanced yield. We estimate that the nitrogen fixation rate by bolide impacts varied from 7×10^{-4} to 2×10^{-3} g N·Myr^{-1}·cm^{-2} and could imply fluvial concentration to explain the nitrogen (1.4 ± 0.7 g N·Myr^{-1}·cm^{-2}) detected as nitrite (NO_2^-) and nitrate (NO_3^-) by Curiosity at Yellowknife Bay. One possible explanation is that the nitrogen detected in the lacustrine sediments at Gale was deposited entirely on the crater's surface and was subsequently dissolved and transported by superficial and ground waters to the lake during favorable wet climatic conditions. The nitrogen content sharply decreases in younger sediments of the Murray formation suggesting a decline of H_2 in the atmosphere and the rise of oxidizing conditions causing a shortage in the supply to putative microbial life.

Plain Language Summary Climate models are able to warm early Mars when CO_2 sources were strong but fail at later times when liquid water still flowed on the surface. A possible solution for the climate puzzle is the presence of abundant H_2 arising from volcanic emissions that could have kept the planet from freezing. H_2 could have also played a key role in the chemistry of the atmosphere. Curiosity discovered the presence of nitrites and nitrates, forms of fixed nitrogen that are required for the origin and sustainability of life in sediments in Gale crater. Here we present theoretical and experimental data that quantify the conversion of molecular nitrogen into fixed nitrogen in the presence and absence of H_2 by the entry shocks of asteroids in the Martian atmosphere and surface. Fixed nitrogen was originally deposited on the surface of Gale crater and then transported to the lake during favorable wet climatic conditions. We found that H_2 is required to yield sufficient fixed nitrogen to explain its detection. The levels of fixed nitrogen sharply

dropped in younger sediments suggesting a decline of H_2 in the atmosphere and the rise of oxidizing conditions causing a nitrogen crisis to putative microbial communities.

1. Introduction

The presence of fluvial landforms on the Martian surface provides indirect evidence that an active hydrological cycle took place at the early stage of evolution of the planet (Luo et al., 2016). This implies that the atmosphere was denser and contained greenhouse gases that allowed a wet and warmer climate. The chemical composition of the early Martian atmosphere is uncertain. Carbon dioxide (CO_2) is generally believed to be the principal gas from the Pre-Noachian (4500 to 4100 Myr) to the Noachian when the young Sun was fainter by ~30% (Gough, 1981). It is estimated that between 0.1 and 3 bars of CO_2 were outgassed during planetary accretion (Kahn, 1985). Climate models required 1–5 bars of CO_2 to keep Mars from freezing (Pollack et al., 1987). Nevertheless, CO_2 escaped to space by photochemistry (Hu et al., 2015), sputtering (Johnson & Liu, 1998), and impact erosion (Melosh & Vickery, 1989; Pham & Karatekin, 2016) as well as sequestered as carbonates (CO_3^{2-}) by surface weathering (Tomkinson et al., 2013). A dense atmosphere (0.5–1 bar) could have persisted from the Pre-Noachian to the Noachian only if atmospheric CO_2 was being continuously resupplied by recycling of CO_3^{2-} by volcanism (Grott et al., 2011; Pollack et al., 1987) and impact degassing (Carr, 1989). As the CO_2 levels dropped below 1 bar, climate models that consider only CO_2 and water are incapable to heat up the Noachian and Hesperian periods in the proximity of the freezing point of water (Wordsworth, 2016). Furthermore, geochemical evidence from sedimentary rocks in Gale crater reveals aqueous alteration but a lack of CO_3^{2-} minerals, suggesting very low levels of CO_2 (0.01–0.1 bar) at the time of deposition, around 3500 Myr ago (Bristow et al., 2017). A possible solution for the Martian climate puzzle is the presence of 10–20% molecular hydrogen (H_2) from volcanic emissions that would have warmed the atmosphere episodically by collision-induced absorption with CO_2 (Ramirez et al., 2014; Sagan, 1977; Wordsworth et al., 2017) or N_2 (Wordsworth & Pierrehumbert, 2013). The total inventory of N_2 in the Martian atmosphere is estimated to range from 0.03 to 0.3 bar (McKay & Stoker, 1989). If N_2 found in the atmosphere of Venus is scaled to Mars, the total inventory of N_2 increases to 0.5–0.6 (von Paris et al., 2013). Such levels of N_2 would have also provided additional warming of the atmosphere by pressure broadening and collision-induced N_2-N_2 absorption (von Paris et al., 2013). Using the size distribution of ancient craters as a proxy for paleopressure, it is inferred that Mars had a total pressure of 0.9–1.9 bars around 3600 Myr ago (Kite et al., 2014).

In addition to its greenhouse effect, H_2 may have had a role in N fixation, for example, the conversion of N_2 into fixed forms of N, such as NO_3^- and hydrogen cyanide (HCN). The key parameters determining the type of N species formed and their rates of fixation are the ratios of carbon (C), oxygen (O), and hydrogen (H) atoms in the atmosphere (Chameides & Walker, 1981; Navarro-González, McKay, & Nna Mvondo, 2001; Stribling & Miller, 1987): for instance, a methane- and H_2-rich atmosphere (high C and H) produces reduced forms of fixed nitrogen, such as HCN, while neutral (CO_2) or oxidized atmospheres (O_2) generate oxidized forms of fixed nitrogen, such as NO. N is a necessary element for life and is frequently inaccessible to microbial communities as it is present in the kinetically inert state, as N_2 in the atmosphere (Postgate, 1996). Because the energy required to break the triple bond in N_2 is high, N fixation, is kinetically limited in spite of being thermodynamically favorable (Howard & Rees, 1996). Therefore, processes that transform N_2 into biologically accessible chemical forms, such as NO_3^-, restrict the supply of N to microorganisms. The N fixation was probably triggered by volcanic lightning, ultraviolet light, and bolide impacts on early Mars (Manning et al., 2009; Segura & Navarro-González, 2005), but the role of H_2 has not yet been explored. So far the Sample Analysis at Mars (SAM) instrument suite of the NASA Mars Science Laboratory (MSL) has discovered the presence of NO_3^- in Hesperian sediments along a stratigraphic transect investigated by the Curiosity rover at Gale crater (Ming et al., 2014; Navarro-González et al., 2013; J. C. Stern et al., 2015, 2017, 2018; Sutter et al., 2017); the origin of NO_3^- is thought to be from the shocks of bolide impacts (J. C. Stern et al., 2015).

In this study we present experimental data and theoretical calculations that investigate the efficiency of shocks from bolide impacts for N fixation in atmospheres (1 bar) containing different $CO_2/(CO_2 + N_2)$ ratios with or without H_2. These values are used to derive the lower and upper boundaries of the N fixation rate by

Journal of Geophysical Research: Planets

AGU
100
ADVANCING EARTH
AND SPACE SCIENCE

10.1029/2018JE005852

bolide impacts. In addition we have reexamined the SAM data to search for the presence of NO_2^- and NO_3^-, determine the amount of fixed nitrogen present in the stratigraphic sequence investigated by the Curiosity rover up to date, and estimate the N deposition rate. The rate of N fixation by bolide impacts and other forms of energy are examined to account for the supply of the observed N deposition at Gale crater.

2. Materials and Methods

2.1. Theoretical Estimate of NO

The equilibrium concentrations of N, O, NO, and N_2 as a function of temperature were calculated using a computer program that models chemical speciation at thermodynamic equilibrium (Bale et al., 2016). The program predicts the chemical species and their mixing ratios that are in thermochemical equilibrium at a given temperature and pressure (1 bar) based on the chemical composition of the initial gas mixture. The rates of reactions as a function of temperature were obtained from the National Institute of Standards and Technology Chemical Kinetics Database (Manion et al., 2015).

2.2. Preparation of Simulated Atmospheres

Simulated atmospheres of different composition containing CO_2 (99.8% purity), N_2 (99.998% purity), and H_2 (99.999% purity) were prepared using a computerized gas-blending system equipped with eight gas lines regulated by high accuracy and fast response mass flow controllers that operate with a maximum rate of 20 cm^3/min at 4 bars. Each gas tank is connected to a two-stage regulator, a particle filter (2 μm), and stainless steel tubing. At the end of the line there is a pneumatic switch valve connected to the mass flow control and a check valve which merges into a 4-L stainless steel container for filling up the simulated atmosphere and which restricts the backflow of the gases preventing contamination of the gas lines. The gas-blending system was connected into a manifold gas line with vacuum, pressure, and temperature meters. The gas-blending system and the manifold were evacuated to 8.6×10^{-3} mbar before opening the gas cylinder valves. Finally, the gas-blending system was filled to 4 bars (value restricted by the operation of the mass flow control modules) with the desired atmosphere in about 8 hr. Once the simulated atmosphere was ready for use, it was transferred into previously vacuum-evacuated round borosilicate (Pyrex) reactors of 1-L capacity equipped with high vacuum stopcocks and filled to 1 bar at room temperature (21 °C).

2.3. Simulation of Bolide Impacts

The effect of bolide impacts were simulated in the laboratory by shocks created under a controlled atmosphere by concentrating a pulsed Nd:YAG laser beam of 1.06 μm photons inside a closed Pyrex reactor of 1-L capacity at 1 bar using a planoconvex optical glass lens with antireflecting coating with a positive focal length of 10 cm and a focal aberration of ~10 μm. Laser-induced plasmas have been extensively used to study the effect of shock waves in planetary atmospheres (Managadze et al., 2003; McKay & Borucki, 1997; Scattergood et al., 1989). When the electric field of the infrared laser radiation becomes greater than that of the binding electrons to their nuclei near the focus point of the lens, it triggers breakdown of the gas molecules. This electric breakdown causes a cascade effect because the ionized gas becomes very absorbent to the laser light so that more of the energy is absorbed (Panarella, 1974). The plasma generated in our facility using air under similar experimental conditions was found to reach a temperature near 17000 K and creates a shock wave with initial velocity of >60 km/s at 20 ns, as determined by interferometry and shadowgraphy techniques (Sobral et al., 2000). Essentially this method is equivalent to a piston-free shock tube with the advantage of conducting the experiment on a tabletop setup with a good controllability of a small explosion in a variety of confined atmospheres (Sasoh, 2016). The laser beam had an energy of 250 mJ per pulse in 5–7 ns operating at 10 Hz. The laser beam is not absorbed completely by the gas mixture in producing the plasma. It was found that between 20% and 30% of the energy was transmitted out of the reactor. The energy absorbed in the production of the plasma was calculated by eliminating the energy transmitted by the plasma in the direction opposite of the incoming laser beam and was measured with an optical power system (Labmaster Ultima, Coherent) using an optical sensor (LM-P10). The reactors were exposed from 0 to 30 min at intervals of 5 min.

2.4. Gas Chromatography Coupled to Mass Spectrometry Analysis

NO was analyzed by gas chromatography (GC)-mass spectrometry (MS) using electron impact ionization. The irradiated atmosphere was introduced into the injection port of an Agilent Technologies 7890A GC

system held at 250 °C by an automatic six-port gas-sampling valve connected to a gas manifold with a vacuum line, a gas sampling port, and a stainless steel loop of 5 ml capacity for sample injection. A styrene-divinylbenzene-based porous polymer column was used (CP-Porabond Q fused-silica) of 50 m × 0.32 mm I.D. with a 5-μm polymer thickness coating. The chromatographic separation was carried out using a program temperature that was initially kept at 50 °C for 5 min and then increased at rate of 10 °C/min until a final temperature of 240 °C, which was held for 6 min. Helium was used as the carrier gas with a flow of 1.2 ml/min. The sample split ratio was 1:100. The GC was interfaced at 250 °C with a mass detector (Agilent Technologies 5975C inert XL EL/CI MSD with Triple Axis detector). The mass spectrometer operated in scan mode from 10 to 150 m/z with a mass resolution of 0.1 amu using electron impact ionization mode at 70 eV. The temperature zones of the ion source and the quadrupole were kept at 230 and 150 °C, respectively. NO was identified by its retention time and its characteristic fragmentation pattern in MS: NO^+ (100%), N^+ (7.5%), O^+ (1.5%), and NO^{2+} (2.4%). Nitrous oxide (N_2O) was detected in low yield, representing ≤0.06% of the NO signal, and was therefore not surveyed. Nitrogen dioxide (NO_2) was not observed in the experiments. Reduced forms of nitrogen were not detected in the experiments, such as ammonia (NH_3), HCN, acetonitrile (CH_3CN), and cyanoacetylene ($HC \equiv C\text{-}CN$). These oxidized or reduced forms of nitrogen are resolved chromatographically into individual peaks (Do & Raulin, 1989; Nna Mvondo et al., 2001) and have sensitivities similar to or slightly higher than NO taking into account their ionization cross sections.

2.5. NO Calibration

A calibration curve of NO was constructed from the analysis of 10 gas mixtures of NO (18 to 4,036 ppm in N_2) that were prepared using the computerized gas-blending system described above using two NO calibration standards (390 and 4,036 ppm in N_2).

2.6. SAM-Like Laboratory Experiments

Several mixtures of NO_2^- or NO_3^- salts (10%) were mixed with different oxychlorine species (90%) in the form of chlorates (ClO_3^-) or perchlorate (ClO_4^-) salts. The chemicals used were reagent grade: $NaNO_3$ (Sigma Aldrich, >99.99%), KNO_3 (Química Meyer, >99.0%), Mg $(NO_3)_2$ (Fluka, >99.0%), Ca $(NO_3)_2$ (Sigma Aldrich, >99.0%), Fe $(NO_3)_3$ (Sigma Aldrich, >98.0%), $NaNO_2$ (J. T. Baker, >98.6%), $NaClO_4$ (Sigma Aldrich, >98.0%), $KClO_4$ (Sigma Aldrich, >99.0%), Mg $(ClO_4)_2$ (Sigma Aldrich, 99.0%), Ca $(ClO_4)_2$ (Sigma Aldrich, 99.0%), Fe $(ClO_4)_2$ (Sigma Aldrich, >98.0%), Fe $(ClO_4)_3$ (Sigma Aldrich, <0.1 chloride content), and synthesized Mg $(ClO_3)_2$ and Ca $(ClO_3)_2$. Mg $(ClO_3)_2$ was not commercially available and was synthesized by mixing stoichiometric ratios of magnesium sulfate ($MgSO_4$ anhydrous, Sigma-Aldrich, 99.5%) and barium chlorate (Ba $(ClO_3)_2 \cdot 2H_2O$, Sigma-Aldrich, 98.0%) according to the method used by Hanley et al. (2012). Ba $(ClO_3)_2$ was dissolved in bidistilled water on a stirplate, and then $MgSO_4$ was slowly added. Since $BaSO_4$ is highly insoluble, it quickly precipitated out of solution as a white solid, leaving behind Mg^{2+} and ClO_3^- in solution. The clear solution was decanted and filtrated through a 20- to 25-μm filter paper. Then it was centrifuged twice to separate the residual $BaSO_4$, and finally it was freeze-dried obtaining a solid powder. Ca $(ClO_3)_2$ was not commercially available, too, and was prepared using the same method by replacing magnesium sulfate for calcium sulfate ($CaSO_4$ anhydrous, Sigma-Aldrich, 99.0%). The purity of the synthesized Mg $(ClO_3)_2$ or Ca $(ClO_3)_2$ was confirmed by thermal analyses carried out by simultaneous measurements of thermogravimetric analysis and differential scanning calorimetry (DSC) coupled to evolved gas analysis by MS in the temperature range from 30 to 1450 °C.

The mixtures of NO_2^- or NO_3^- salts mixed with different oxychlorine species (ClO_3^- or ClO_4^-) were analyzed in the laboratory under SAM-like conditions in order to facilitate the interpretation of the Mars data. Thermal analyses were carried out by simultaneous measurements by thermogravimetric analysis-DSC-MS that was configured to operate under SAM-like conditions (Mahaffy et al., 2012). The instrument used was a Netzsch STA 449 F1 Jupiter thermobalance (TG-DSC/DTA Apparatus) utilizing two furnaces made of steel or silicon carbide operating in the temperature range from −150 to 1550 °C which was interfaced to a Netzsch mass spectrometer QMS 403 C Aëolos. The sample was ground and sieved to <75 μm using an agate pestle and mortar set, and a portion (~15 mg) was introduced into alumina (Al_2O_3) crucibles. An identical empty alumina crucible was used as reference material. The thermal analysis was carried out using the silicon carbide furnace that was heated from 30 to 850 °C at a rate of 35 °C/min. A nitrogen flow of 2 cm^3/min was

used to transfer the evolved gases out of the thermobalance using an oven pressure of 35 mbar. The evolved gases were scanned by MS from 14 to 120 m/z using electron impact ionization mode operated at 70 eV.

2.7. Martian Samples

Curiosity has drilled 12 (1.6-cm diameter, 6 cm deep) lacustrine mudstones during its traverse from the landing site at Bradbury at the lowest stratigraphic layers encountered on Aeolis Palus to the upper strata of the base of Aeolis Mons (see Figure 4): John Klein (Sol 182, 8 February 2013) and Cumberland (Sol 279, 19 May 2013) from the Yellowknife Bay formation, and Confidence Hills (Sol 759, 24 September 2014), Mojave (Sol 882, 29 January 2015), Telegraph Peak (Sol 908, 24 February 2015), Buckskin (Sol 1060, 30 July 2015), Oudam (Sol 1361, 4 June 2016), Marimba (Sol 1422, 6 August 2016), Quela (Sol 1464, 18 September 2016), Sebina (Sol 1495, 20 October 2016), Duluth (Sol 2057, 20 May 2018), and Stoer (Sol 2136, 8 August 2018) from the Murray formation. In addition, it has also drilled a sandstone in the Kimberley formation known as Windjana (Sol 621, 5 May 2014) composed primarily of fluvial conglomerate and deltaic sandstone (see Figure 4). Finally, it has also drilled four eolian sandstones of the Stimson formation that unconformably lie above the Murray formation (see Figure 4, main text): Big Sky (Sol 1119, 29 September 2015), Greenhorn (Sol 1137, 18 October 2015), Lubango (Sol 1320, 23 April 2016), and Okoruso (Sol 1332, 5 May 2016). The samples Lubango, Okoruso, and Sebina were not analyzed by SAM. The sampling sites have been described in detail elsewhere (Hogancamp et al., 2018; J. C. Stern et al., 2017).

2.8. SAM Measurements

The SAM instrument suite has been described in detail previously (Mahaffy et al., 2012). SAM is positioned in the front body of the rover and receives samples that have been drilled and then processed on the end of Curiosity's robotic arm (Anderson et al., 2012). The analyses were carried out under the so-called "nominal solid-sample analysis mode." Prior to a sample run, a single-quartz cup was preheated to >800 °C under He flow with active pumping using SAM's wide-range pumps to eliminate volatiles and potential contaminants that were previously absorbed. Then the cup was rotated to be positioned underneath the SAM solid sample inlet tube to acquire the sample from the Collection and Handling for In-Situ Martian Rock Analysis (CHIMRA) device. The rock powder was sieved (<150 μm) and delivered in single (~76 mm^3), triple, or quadruple aliquots into one of SAM's cups. Once the sample was received, the cup was hermetically sealed and moved inside the SAM pyrolysis oven. The sample cup contains a porous quartz frit on the bottom where a stream of helium (~0.8 cm^3/min) flows vertically through the sample for efficient transport of evolved gases out of the oven during the heating process. The sample was heated from Mars ambient temperature to ~870 °C at heating rate of 35 °C/min, maintaining an oven pressure of ~25 mbar during the analysis. The evolved gases were continuously analyzed by a quadrupole mass spectrometer operating with electron impact ionization mode at 70 eV.

The ion with a mass to charge ratio (m/z) of 30 was selected to monitor and quantify NO, which is the major product of thermal decomposition of nitrate. NO evolved at temperatures that was characteristic for the thermal decomposition of NO_3^- or mixtures of NO_3^- and ClO_4^-. NO_2^- also thermally decomposes releasing NO, but no studies were previously available to determine their presence in the Martian samples. Other plausible interferences on m/z 30 include an isotopologue of CO, $^{12}C^{18}O$ arising from the electron impact ionization of CO and CO_2; however, the m/z 30 signal represents 0.2%, and 0.04% of the m/z 28 signal arising from the electron impact ionization of CO and CO_2, respectively. Even if CO_2 was released in large quantities in the Martian samples, the contribution of $^{12}C^{18}O$ to the m/z 30 signal is negligible (<1%). N-methyl-N-(tert-butyldimethylsilyl) trifluoroacetamide, abbreviated as MTBSTFA, is a derivatization agent that was brought to Mars in sealed cups for wet chemistry SAM-GCMS analysis. Nonetheless, one cup was found to leak and reacted with the samples during nominal solid-sample analysis mode leading to the detection of hydrocarbons and NO (Freissinet et al., 2015; Glavin et al., 2013; J. C. Stern et al., 2015; Sutter et al., 2017). The interference of MTBSTFA in the NO measurement by SAM was calculated by the background correction method by J. C. Stern et al. (2015). Since each molecule of MTBSTFA has one N atom that can potentially decompose into NO, its contribution can be subtracted from the total amount of NO measured in the SAM experiments. This method was used to calculate the nitrogen content in the drilled samples from John Klein up to Greenhorn (J. C. Stern et al., 2015, 2017). In order to decipher if nitrites are present in the Martian samples, it is required to know the thermal evolution profiles of NO from nitrites and nitrates. In this scenario, it is not possible to use the background correction method. Instead, it is required to
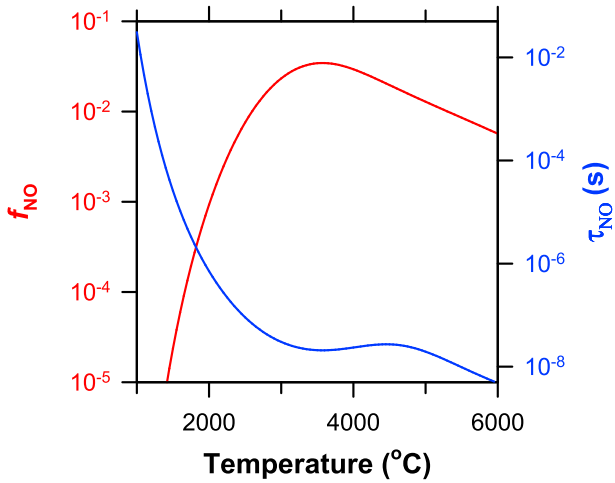
Figure 1. The NO equilibrium mixing ratio (f_{NO}) and the relaxation time for NO (τ_{NO}) as a function of temperature. f_{NO} is expressed as the number of moles of NO divided by the total number of moles of all gas constituents in a mixture composed of 50% CO2 and 50% N2 without H2 at 1 bar.

eliminate the m/z 30 signal of MTBSTFA products as they thermally evolve during the analysis. Laboratory experiments of MTBSTFA degradation products under SAM-like conditions indicate that the major interferences to the m/z 30 signal are formaldehyde (HCHO, m/z 29 [100%] and m/z 30 [~60%]) and ethane (C_2H_6, m/z 29 [~20%] and m/z 30 [~20%]). Therefore, it is possible to eliminate their contribution according to the following empirical formula:

$$NO\ signal = m/z\ 30 - b(m/z\ 29 - m/z\ 43)$$

where b is a constant that varies from 0.6 (contribution from HCHO) to 0.8 (contributions from both HCHO and C_2H_6) and even to 1.0 (contributions from HCHO, C_2H_6, and unidentified species) depending on the run. The m/z 43 signal is attributed to ketones, alkyladehydes, and/or hydrocarbons. Supporting information Figures S1 through S14 show the signals for m/z 29, 30, and 43 and the resultant NO profiles for all the samples investigated. These plots were dead time and background corrected.

The nitrogen content in the Martian samples was calculated from the NO signal that was corrected taking into account its ionization cross section at 70 eV relative to the response of CO_2 in the sample, for which a calibration curve exists (Archer et al., 2014). The error reported for a single run includes the error in the determination of the area of NO and the uncertainty in the mass of the sample delivered to SAM. For multiple sample analysis the error reported was the mean and standard deviation (1σ) of the measurements.

3. Results and Discussion

3.1. Theoretical and Experimental Production of NO by Shock Waves

The theoretical estimate for the production of NO takes into account that NO is formed at high temperature as the air is suddenly heated by the shock wave. The concentration of NO rapidly reaches thermochemical equilibrium with the temperature of the surrounding gas. As the shocked air expands and cools, a point in time is reached when thermochemical equilibrium is no longer kept during the rapid cooling process and a net amount of NO is "frozen" at a given temperature (Chameides et al., 1977). The formation of NO in shock-heated $CO_2/(CO_2 + N_2)$ atmospheres occurs at temperatures in excess of 2000 K (Navarro-González, McKay, & Nna Mvondo, 2001) and is initiated by the reaction of atomic oxygen (O), arising from the dissociation of CO_2, with N_2 via reaction (R1):

$$O + N_2 \leftrightarrows NO + N. \tag{R1}$$

This reaction is part of the Zel'dovitch mechanism for the oxidation of N_2 in air (Zel'dovitch & Raizer, 1966). As the shock wave expands and the gas cools, the NO equilibrium mixing ratio (f_{NO}) changes with temperature (Figure 1); f_{NO} is locked at a characteristic temperature, usually referred to as the freeze-out temperature (T_F), when the relaxation time of NO (τ_{NO}) becomes equal to or greater than the cooling time of the heated gas (Chameides et al., 1977). f_{NO} and the equilibrium concentrations of N, O, NO, and N_2 were calculated as a function of temperature; τ_{NO} was determined using the rate constants (k) for the forward (f) and reverse (r) pathways of reaction (R1). The relaxation time of NO (τ_{NO}) to establish equilibrium conditions to a drop in temperature as the air expands and cools is given in equation (1):

$$\tau_{NO} = \frac{1}{k_f([O] + [N_2]) + k_r([NO] + [N])}; \tag{1}$$

where [O], [N], [NO], and [N_2] are the equilibrium concentrations before the temperature change, and k_f and k_r are the rates of reactions at the jump down temperature. The rates of reactions as a function of temperature are $k_f = 3.0 \times^{-10} cm^3 \cdot molecule^{-1} \cdot s^{-1}\ e^{-(318.0\ kJmole^{-1}/RT)}$ and $k_r = 7.1 \times^{-11} cm^3 \cdot molecule^{-1} \cdot s^{-1}$ $e^{-(6.6\ kJmole^{-1}/RT)}$ (Manion et al., 2015).
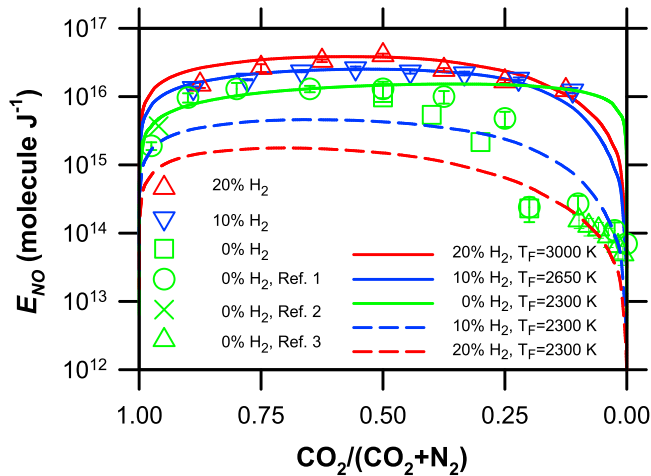
Figure 2. Variation of E_{NO} as a function of the $CO_2/(CO_2 + N_2)$ mole ratio in shock waves simulating different possible compositions of the primitive Martian atmosphere at 1 bar. Symbols are experimental data, and lines are predictions. Ref. 1 = Navarro-González, McKay, and Nna Mvondo (2001); Ref. 2 = Levine et al. (1982); Ref. 3 = Navarro (2014).

Figure 1 also shows how the relaxation time varies with temperature. T_F can vary depending on the instantaneous energy input delivered to produce the shock wave; for example, more energy results in faster cooling time of the heated gas (Chameides, 1979) and the chemical composition of the gas mixture (Chameides & Walker, 1981). The energy yield for the production of NO produced by bolide impacts was estimated from a revised version of the model of Chameides et al. (1977), in which about 50% of the energy of the impact was dissipated by the shock wave in the form of heat, and the Cp for the gases in the mixture were taken into account, according to the following equation (equation (2)):

$$E_{NO} = \frac{0.5 \times N_A \times f_{NO}(T_F)}{T_F \times ([CO_2]Cp_{CO_2} + [N_2]Cp_{N_2} + [H_2]Cp_{H_2})}; \qquad (2)$$

where E_{NO} refers to the number of NO molecules that formed per joule absorbed; N_A is the Avogadro constant; $f_{NO}(T_F)$ is the predicted nitric oxide equilibrium mixing ratio at T_F; [gas] is the mole fraction of each gas in the mixture; and Cp is the specific heat at constant pressure of each gas. T_F and f_{NO} were not actually measured experimentally, but T_F was left as a free parameter to adjust the experimental value of E_{NO} with that computed using equation (2).
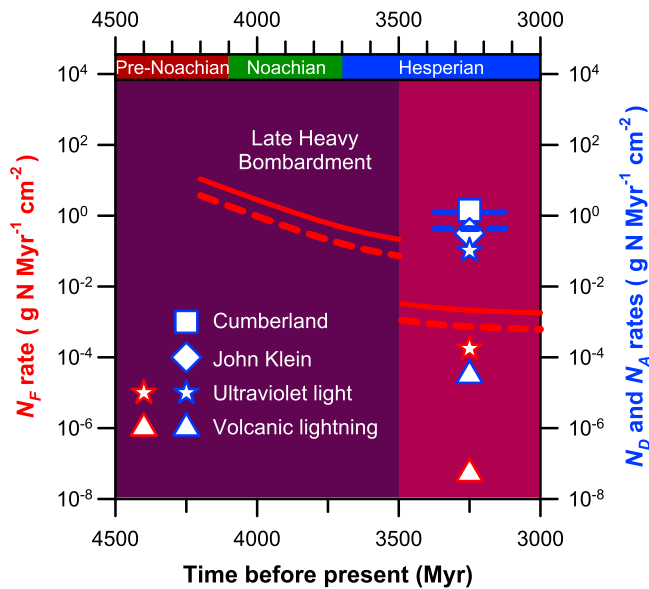
Shock waves in the laboratory were generated by focusing a pulse laser inside a reactor with simulated atmospheres (CO_2, N_2, and H_2) at 1 bar (Navarro-González, Villagrán-Muniz, et al., 2001; Sobral et al., 2000). The presence of H_2 was expected to lead to the fixation of reduced forms of N, such as HCN and HC $\equiv$ C-CN. Surprisingly, none of these species were detected. The net amount of NO produced in the experiments was determined by GC coupled to MS, and the energy deposited was determined optically. E_{NO} was derived from the slope of a linear plot of the number of molecules formed as a function of the energy absorbed in the experiments (Navarro-González, McKay, & Nna Mvondo, 2001). E_{NO} has been found to vary linearly with pressure (Rahman & Cooray, 2008).

Tables S1 and S2 and Figure 2 show how the experimental and predicted energy yields for the production of NO by shock waves vary with the $CO_2/(CO_2 + N_2)$ ratio in different simulated primitive Martian atmospheres in the absence and presence of 10% and 20% H_2. It also includes data from previous experiments (Levine et al., 1982; Navarro, 2014; Navarro-González, McKay, & Nna Mvondo, 2001) in the absence of H_2. In particular, the experimental data at 0% H_2 indicate that the formation of NO increases from ~1.9×10^{15} molecules/J at $CO_2/(CO_2 + N_2) = 0.98$ to ~1.3×10^{16} molecules/J at $CO_2/(CO_2 + N_2)$ from 0.8 to 0.5 and then drastically drops to ~4.9×10^{13} molecules/J at $CO_2/(CO_2 + N_2) = 0.01$. The expected T_F for NO in shock-heated air (N_2/O_2) is 2300 K (Navarro-González, Villagrán-Muniz, et al., 2001). The predicted trend using this value is in good agreement with experiments at $CO_2/(CO_2 + N_2) \geq 0.5$. At lower CO_2 levels T_F for NO is probably much lower resulting in a diminishing in the NO yield. Surprisingly there is a 1.7-fold and 2.6-fold increase in the experimental NO energy yield when 10% and 20% H_2 are included in the system, respectively. However, if T_F for NO were to remain constant at 2300 K, the expected NO energy yield would drop off at 69% and 88% in 10% and 20% H_2, respectively. Consequently the discrepancy between experimental data and theoretical trends shown in Figure 2 is due to the appropriate T_F values used in the computations. In order to explain the sudden increase in the NO energy yield when H_2 is included, the T_F for NO must change to 2650 and 3000 K in 10% and 20% H_2, successively. This means that the shock wave cools off much faster in the presence of H_2 when f_{NO} has a higher value resulting in an enhanced amount of NO frozen in the heated gas by the shock wave. This is counterintuitive because H_2 is a reducing agent and was not expect to lead to an enhancement in the rate of nitrogen oxidation. This finding has important implications for the N fixation rate of the Martian atmosphere under reducing conditions.

3.2. The Nitrogen Fixation Rate by Bolide Impacts

The N fixation rate (N_F) was estimated assuming that NO was quantitatively converted to NO_2^- and/or NO_3^- and no losses occurred in either the atmosphere (Mancinelli & Banin, 2003; Summers & Khare,

Figure 3. The nitrogen fixation (N_F) and the nitrogen deposition (N_D) or the nitrogen accumulation (N_A) rates as a function of time in the Martian atmosphere are shown by the red and blue lines and symbols, respectively. The dash and solid lines constrain the lower (0% H_2) and upper (20% H_2) boundaries in $CO_2/(CO_2 + N_2)$ atmospheres by bolide impacts, consecutively. The abrupt change in slopes at 3500 Myr is due to different radius of projectiles during (population 1 = 2 km) and after (population 2 = 0.5 km) the late heavy bombardment process. The stars show the rate by ultraviolet light (after Yung et al., 1977; Smith et al., 2014). The triangles show the rate by volcanic lightning (after Navarro-González et al., 1998; Segura & Navarro-González, 2001, 2005). The square and diamond symbols show N_D rates determined for the Cumberland and John Klein at Yellowknife Bay, in Gale crater assuming a sediment deposition rate of 20,000 cm/Myr (see section 3.5). The N_A rates for bolide impacts, ultraviolet light, and volcanic lightning were calculated assuming that NO_2^- and NO_3^- deposited entirely on the Gale's crater were ultimately transported to the bottom of the lake (see sections 3.5 and 3.6).

2007) or surface due to N_2O (Samarkin et al., 2010). The impactor flux on Mars was used to calculate the N fixation rate through time. This was calculated by using the Hartmann and Neukum (2001) to derive the cumulative number (N) of projectiles producing craters with diameters ≥1 km in an area of 1 km^2 over the entire history of Mars. The analytical description of the model is given by equation (3):

$$N_F = 2.68 \times 10^{-14} \left(e^{(6.93t)} - 1 \right) + 4.13 \times 10^{-4}\, t; \qquad (3)$$

where, t denotes time in billion years. The nature of the planetary objects that impacted early Mars is not known. Analysis of crater size distributions indicates two populations of projectiles (Strom et al., 2005). Population 1 has a radius centered at 2 km (Strom et al., 2005) and was responsible for the late heavy bombardment (LHB): from ~4200 to ~3500 Myr (Bottke & Norman, 2017). The sources of these objects were likely asteroids (Strom et al., 2005) and to a lesser extent comets (Gomes et al., 2005) that were dynamically ejected by orbital migration of the giant planets. Population 2 has a radius centered at 0.5 km, similar in size to the near-Earth asteroids, and was responsible for the impacts (Strom et al., 2005) after the LHB. The mass (m) of projectiles from populations 1 and 2 was calculated using a density of 3 g/cm^3, typical of a basaltic asteroid (Kring & Cohen, 2002). The average impact velocity (v) estimated for Mars is 9.8 km/s (Ivanov, 2001) and was assumed to be similar for both populations of projectiles. The energy deposited into the atmosphere by these two populations of impactors was calculated as $mv^2/2$ (Melosh & Vickery, 1989).

The estimated upper and lower boundaries for the N fixation rate by bolide impacts are given in Table S3, and their trends are shown in Figure 3 from the Pre-Noachian to the Hesperian considering the presence or absence of H_2 in the atmosphere. The abrupt change in the slopes at 3500 Myr is due to the different size of projectiles during and after LHB. The upper boundary ($[CO_2/(CO_2 + N_2)] = 0.5$, and 20% H_2) has a maximum rate of 10.8 g N·Myr^{-1}·cm^{-2} at the start of the LHB in the Pre-Noachian, and then it rapidly decreased to 0.2 g N·Myr^{-1}·cm^{-2} at the end of the LHB at the early Hesperian (Figure 3). During this time the total accumulated mass of nitrogen in the surface is predicted to be 22.4 g N/cm^2, equivalent to a global deposit of *60 cm* of purely solid sodium nitrate ($NaNO_3$). In contrast, the lower boundary ($[CO_2/(CO_2 + N_2)] = 0.5$, and 0% H_2) has a maximum rate of 3.7 g N·Myr^{-1}·cm^{-2} at 4200 Myr ago, decreasing steadily to 0.07 g N·Myr^{-1}·cm^{-2} at the end of the LHB (Figure 3). The total accumulated mass of nitrogen on the Martian surface is predicted to be 7.7 g N/cm^2, equivalent to a global deposit of *20 cm* of purely solid $NaNO_3$. In both scenarios it is possible that a significant fraction of the N fixed may have been destroyed (Manning et al., 2008) or buried (Hartmann et al., 2001) due to resurfacing or gardening during the LHB. After the LHB, the rate of N fixation slowly dropped from 3.3×10^{-3} to 1.8×10^{-3} g N·Myr^{-1}·cm^{-2} and from 1.1×10^{-3} to 6.2×10^{-4} g N·Myr^{-1}·cm^{-2} from the early to the end of the Hesperian for the upper and lower boundaries, respectively (Figure 3). It is predicted that a mass of nitrogen ranging from 4.4 to 12.8 mg N/cm^2 would have been globally deposited on the surface during the Hesperian, equivalent to a deposit of $NaNO_3$ ranging from *12 to 34 mm* for the lower and upper boundaries, correspondingly.

3.3. Fixed Nitrogen Products Detected by MSL

The Phoenix mission landed in the northern plains of Mars on 25 May 2008. It has been the only spacecraft designed to search for soil NO_3^- but was unable to detect any by the Wet Chemistry Laboratory and Thermal and Evolved Gas Analyzer (Hecht et al., 2009). The Wet Chemistry Laboratory was equipped with an ion selective electrode for measuring nitrate from an aqueous extract of Martian soil, but with the unexpected
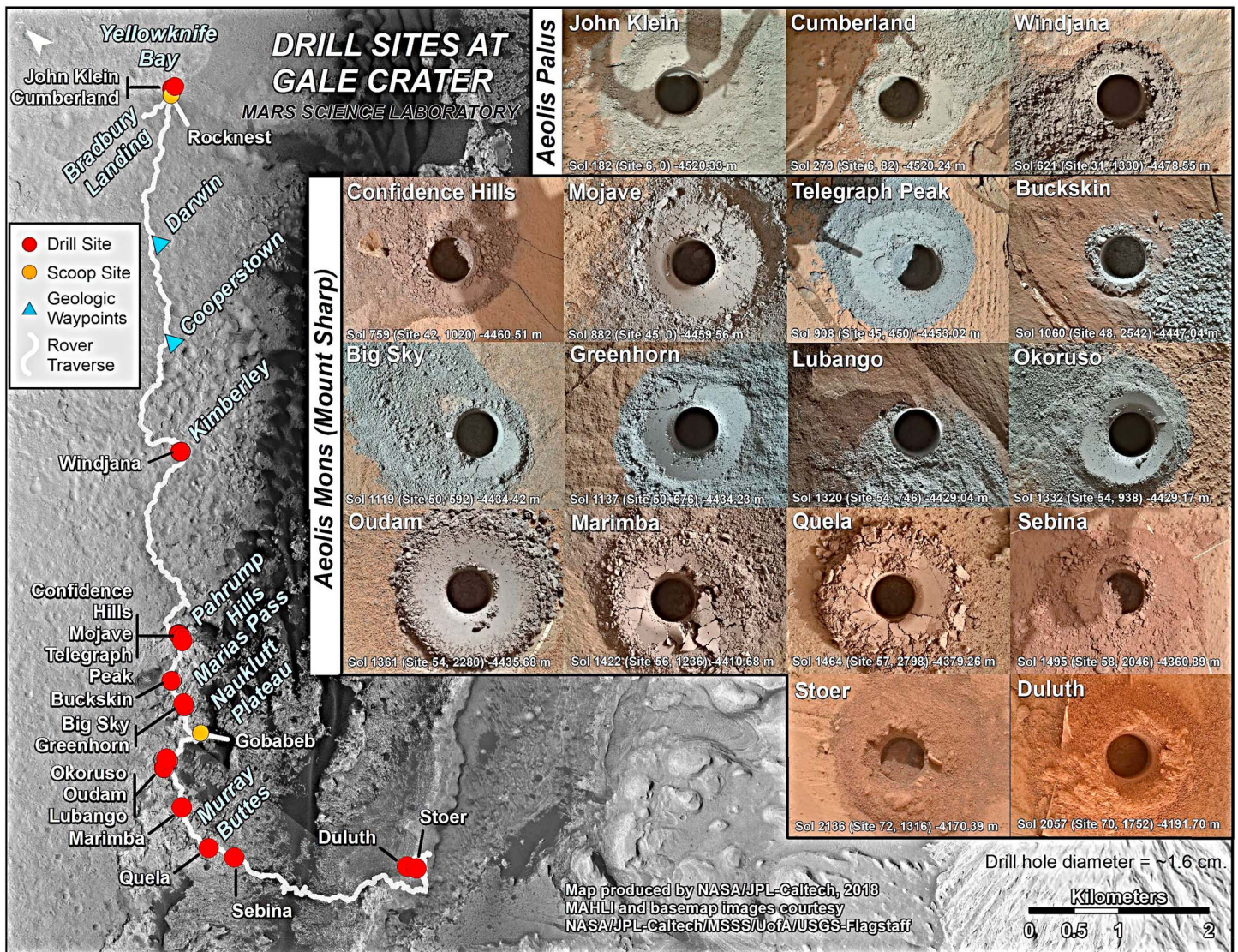
Figure 4. Rocks studied by NASA's Curiosity rover during its three-Martian-year traverse on Gale crater until Sol 2136 (8 August 8 2018). The inset on the right of the base map is a composite image showing the drilled holes performed by Curiosity. The base map shows on the left the rover traverse with the locations of the rocks surveyed (red dots). Upon landing on Aeolis Palus in August of 2012, Curiosity traversed east from the Bradbury landing site to Yellowknife Bay, and then southwest toward Aeolis Mons reaching the base of the mountain on Sol 746. The total driven distance was 19.641 km until Sol 2156 (30 August 2018). North is toward the upper left corner. The scale bar represents 2 km (1.2 miles). The base map is from the High Resolution Imaging Science Experiment camera on NASA's Mars Reconnaissance Orbiter. Drilled hole images were taken with the Mars Hand Lens Imager (MAHLI) camera on the end of the arm from a distance of about 5 cm. The drill holes are ~1.6 cm wide.

presence of perchlorate in the soil, the response of the electrode resulted to be stronger for perchlorate than nitrate by a factor of 1,000. The Thermal and Evolved Gas Analyzer was unable to detect any evolved NO from the thermal treatment of the arctic Martian soil at concentrations below the natural background levels of ^{15}N ≡ ^{15}N present in the N_2 (Yeung et al., 2017), which was used as the carrier gas to transfer the evolved gases from the oven to the mass spectrometer. The first detection of NO_3^- in soils and sediments was carried out by the SAM instrument suite of the MSL Curiosity rover, after landing on Bradbury at Gale crater on 6 August 2012 (Archer et al., 2014; Ming et al., 2014; Navarro-González et al., 2013; J. C. Stern et al., 2015, 2017, 2018; Sutter et al., 2017). NO_3^- thermally decomposes releasing NO which has been used to quantify it in the Martian surface. Curiosity has traversed a total distance of 19.809 km up until Sol 2221 (5 November 2018), and during this time it has drilled 17 sedimentary rocks (see Figure 4). Fourteen of these rock samples have been analyzed by SAM from the lowest stratigraphic unit Sheepbed
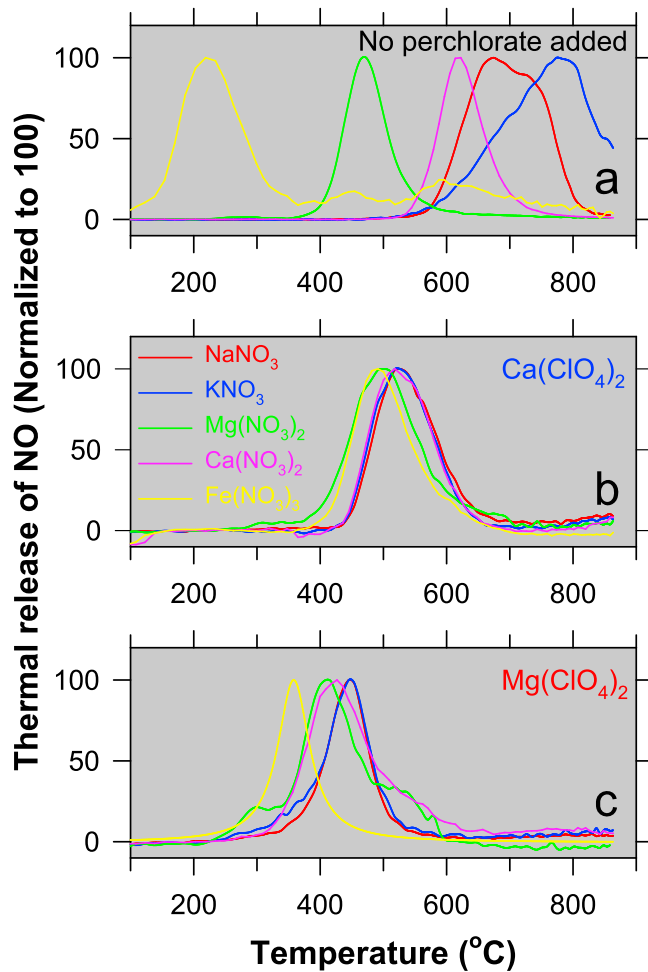
Figure 5. The evolution of NO during the thermal treatment of NaNO$_3$, KNO$_3$, Mg (NO$_3$)$_2$, Ca (NO$_3$)$_2$, and Fe (NO$_3$)$_3$ under Sample Analysis at Mars-like conditions. Panel (a) corresponds to pure nitrates, whereas panels (b) and (c) correspond to mixtures of nitrates (10%) in the presence of calcium and magnesium perchlorate, respectively.

mudstone encountered in Yellowknife Bay to the Murray and Stimson formations located at the base of Aeolis Mons.

When NO$_3^-$ salts are subjected to thermal treatment, they first undergo a phase transition to a liquid state, which are stable to various degrees above their melting points, and then experience decomposition, releasing mainly NO (K. H. Stern, 1972). Figure 5 shows the release of NO for pure salts of nitrates and their mixtures with ClO$_4^-$. Figure 5a shows the thermal behavior for pure nitrates under SAM-like conditions. The thermal stabilities for nitrates increased with the order of Fe (NO$_3$)$_3$ < Mg (NO$_3$)$_2$ < Ca (NO$_3$)$_2$ < NaNO$_3$ < KNO$_3$ and were characterized by the release of NO in a broad temperature range spanning about 150 °C and showing a maximum centered at 225, 475, 622, 675, and 780 °C, respectively. Surprisingly, when these nitrates were blended with ClO$_4^-$, with a molar mixing ratio of 1/9, their thermal stabilities drastically shifted and congregated around a characteristic temperature range spanning from 490 to 530 °C and from 360 to 456 °C, for Ca (ClO$_4$)$_2$ (Figure 5b) and Mg (ClO$_4$)$_2$ (Figure 5c), correspondingly. Such a behavior was first observed by Navarro-González et al. (2013) and is explained by a phase transition from solid to liquid stage of the perchlorates prior to their decomposition (Markowitz & Boryta, 1965). Once the liquid phase is formed, nitrate salts dissolve and exchange their cations between perchlorates and nitrates. This process can take place as soon as either nitrates or perchlorates undergo the phase transition to the liquid stage. This exchange resulted in a shift in the temperature of decomposition for nitrates that is characteristic for each perchlorate salt.

NO$_2^-$ also thermally decomposes in a similar fashion as NO$_3^-$ (K. H. Stern, 1972). We investigated the thermal stability of different nitrates and nitrites in the absence or presence of various perchlorates and chlorates to aid in the identification of these chemical species in the Martian rocks investigated so far (Figure 6). Both NO$_3^-$ and NO$_2^-$ decompose at characteristic temperatures depending on the cation present as shown in Figures 6a and 6b, respectively. The occurrence of perchlorate/chlorates results generally in a reduction in the temperature of decomposition of NO$_3^-$ and NO$_2^-$, and the characteristic temperatures of evolution of NO are determined by the cation present in the oxychlorine species and not in the nitrate or nitrite, as previously discussed. The temperature range shown in these panels corresponds to the lower and higher evolutions of the NO peak signals, as seen in Figures 5b and 5c, which were measured at 75% peak heights for the different nitrates/nitrites studied in the presence of a given perchlorate/chlorate salt. The thermal stabilities of nitrates increased with the order of Fe (ClO$_4$)$_2$ < Fe (ClO$_4$)$_3$ < Mg (ClO$_4$)$_2$ < Ca (ClO$_4$)$_2$ < NaClO$_4$ < K (ClO$_4$) (see Figure 6a). For nitrates mixed with chlorates, their thermal stabilities increased in the same order (Mg (ClO$_3$)$_2$ < Ca (ClO$_3$)$_2$) but were not shifted to lower temperatures as was found in the case for perchlorates (Figure 6a). Nitrates decompose below 300 °C in the presence of Fe (ClO$_4$)$_2$ or Fe (ClO$_4$)$_3$ and above 350 °C in the presence Mg (ClO$_4$)$_2$, Ca (ClO$_4$)$_2$, NaClO$_4$, K (ClO$_4$), Mg (ClO$_3$)$_2$, and Ca (ClO$_3$)$_2$. Figure 6b shows the thermal stabilities of nitrites with perchlorates and chlorates. They show the same thermal stability order as for nitrates except that nitrites decompose below 350 °C in the presence of Fe (ClO$_4$)$_2$, Fe (ClO$_4$)$_3$, Mg (ClO$_4$)$_2$, Ca (ClO$_3$)$_2$, and Mg (ClO$_3$)$_2$, and above 350 °C in the presence of Ca (ClO$_4$)$_2$, NaClO$_4$, and K (ClO$_4$) (see Figure 6b).

Figures 6c and 6d show the NO evolution trends for the different rocks investigated from the lowest sections at JK-BK (Figure 6d) to the highest layers at BS-DL (Figure 6c) labeled by name sequentially across the strata encountered from the Yellowknife Bay to the Stimson formations during the ascent of Curiosity to Aeolis Mons. Surprisingly the samples from lowest layers (JK and CB) showed major releases of NO below 350 °C, and at higher layers, the release of NO gradually shifted to higher temperatures. Most of these
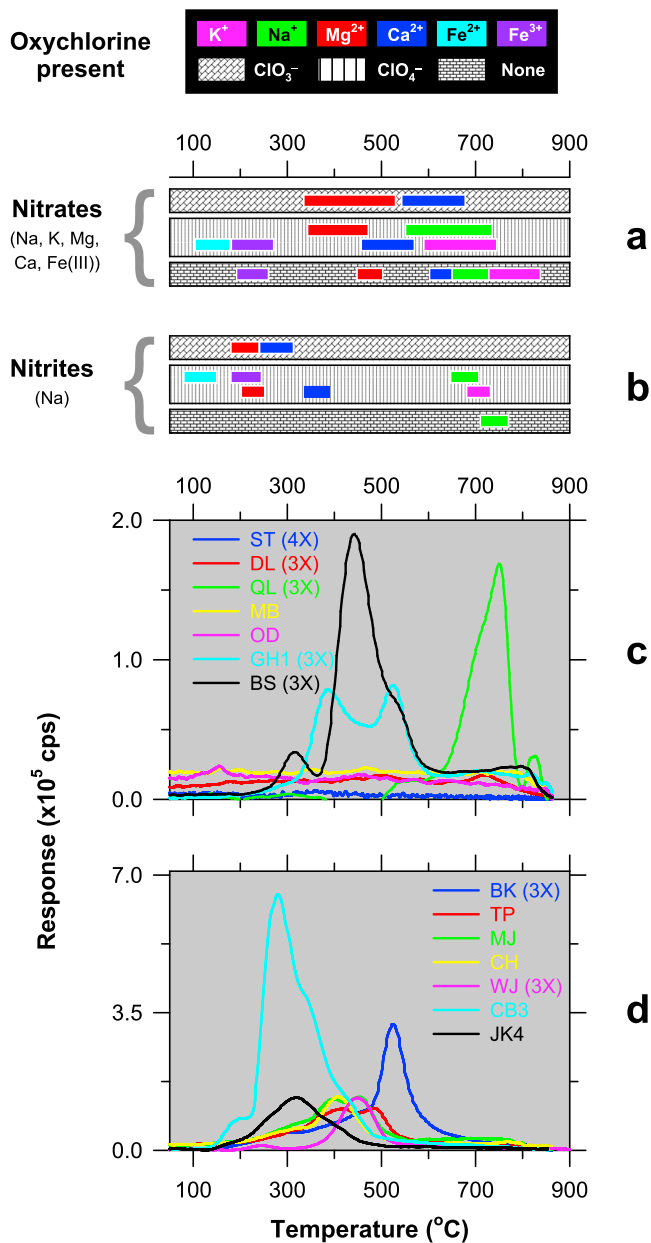
Figure 6. Evolution of NO for the thermal treatment of nitrates (a) and nitrites (b) under SAM-like conditions, and sedimentary facies (c and d) measured by SAM along the stratigraphic column from the Yellowknife Bay to the Stimson formations. The characteristic temperatures for the evolution of NO are shown for pure nitrate (a) or nitrite (b) standards, as well as for the mixtures of nitrates (10%) or nitrites (10%) in the presence of different oxychlorine species (90%) in the form of perchlorates and chlorates (a, b). The sedimentary facies analyzed by SAM from the lower to the upper stratigraphic column: John Klein (JK), Cumberland (CB), Windjana WJ), Confidence Hills (CH), Mojave (MJ), Telegraph Peak (TP), Buckskin (BK), Big Sky (BS), Greenhorn (GH), Oudam (OD), Marimba (MB), Quela (QL), Duluth (DL), and Stoer (ST). The SAM data shown in panels (c) and (d) have been normalized to single portions, and the signals were smoothed using the Savitzky-Golay filter of 25 points. SAM = Sample Analysis at Mars.

samples released oxygen during SAM analyses that suggest the presence of oxychlorine species (Sutter et al., 2017). Their concentrations were higher than for fixed nitrogen species with a (nitrate or nitrite)/oxychlorine mixing ratio from 0.06 to 0.49 (J. C. Stern et al., 2017). The oxygen evolution temperatures are lower than what is typical of perchlorates (Sutter et al., 2017) and appear to be more consistent with $Mg (ClO_3)_2$ and $Ca (ClO_3)_2$ (Sutter et al., 2017) or ClO_3^-/iron phases (Hogancamp et al., 2018). Consequently, NO evolved below 350 °C in the Martian samples could be assigned to NO_2^- and iron-NO_3^-, and above 350 °C to NO_3^-.

3.4. Altitudinal Variation of Fixed Nitrogen at Gale Crater

Figure 7a and Table S4 show the variation of amount of fixed nitrogen present in the lacustrine mudstones and sandstone, as well as the eolian sandstones surveyed by SAM (Figures 6c and 6d) from the lowest to the highest stratigraphic column encountered by the Curiosity rover. Curiosity typically drilled a new rock up in the stratigraphic column every 40 m or less in height depending on the interest of the horizon. However, there was no drilling activity between −4,379 and −4,191 m due to a failure of the drill. The point-to-point plot shows evidence of three distinct episodes centered at −4,436, −4,447, and −4,520 m, respectively, where the concentration of fixed nitrogen reached maximum values and their intensity increased with depth. The peak with the highest levels corresponds to the Cumberland sample at Yellowknife Bay with a concentration of 71 ± 37 µg N/cm^3, a mudstone obtained from a fluvio-lacustrine strata at the Sheepbed member, which is an embayment on the floor of Gale crater. Multiple portions of this sample were analyzed several times, and the amount of fixed nitrogen detected exhibited high variability (see Table S4). Similar dispersion was observed for other volatiles present in different runs for the sample (Ming et al., 2014). A plausible explanation is that it was not well homogenized when supplied to SAM. The John Klein sample was drilled only 3 m away in the Sheepbed mudstone and within ~0.1 m of the same stratigraphic location (Ming et al., 2014). This sample showed lower levels of fixed nitrogen (16 ± 7 µg N/cm^3), possibly because it was leached due to postdepositional aqueous alteration as evidenced by the presence of calcium sulfate veins. The levels of fixed nitrogen declined to ~10 ± 3 µg N/cm^3 for the Widjana sample extracted from a sandstone outcrop of likely eolian origin that occurs about 40 m above the Sheepbed mudstone samples (Sutter et al., 2017). The second less intense peak corresponds to the sample obtained from the Buckskin outcrop, with a value of 35 ± 8 µg N/cm^3. This mudstone contains tridymite, a SiO_2 mineral that forms in environments dominated by high-temperature magmas enriched in silica, and consequently its presence provides evidence for silicic volcanism in Mars (Morris et al., 2016). The concentration of fixed nitrogen decreases up in the stratigraphy in sediments associated with episodic lake drying (Bristow et al., 2018). The first sample where NO_2^- and/or NO_3^- were not detected corresponds to Marimba (−4,411 m), drilled from a ~30-m-thick structure composed of finely laminated mudstones of the Karasburg member, which indicates the resume of subaqueous deposition (Bristow et al., 2018). The third peak with the lowest levels of fixed nitrogen (8 ± 4 µg N/cm^3) corresponds to Quela, a mudstone drilled ~31 m above Marimba in the same geologic formation. Curiosity did not drill after Sol 1537 due to a mechanical issue that took the drill offline in December 2016. The first drill site after the drill problem had been solved was Duluth that is situated ~188 m above Quela, near Vera Rubin Ridge with high concentration of hematite. This
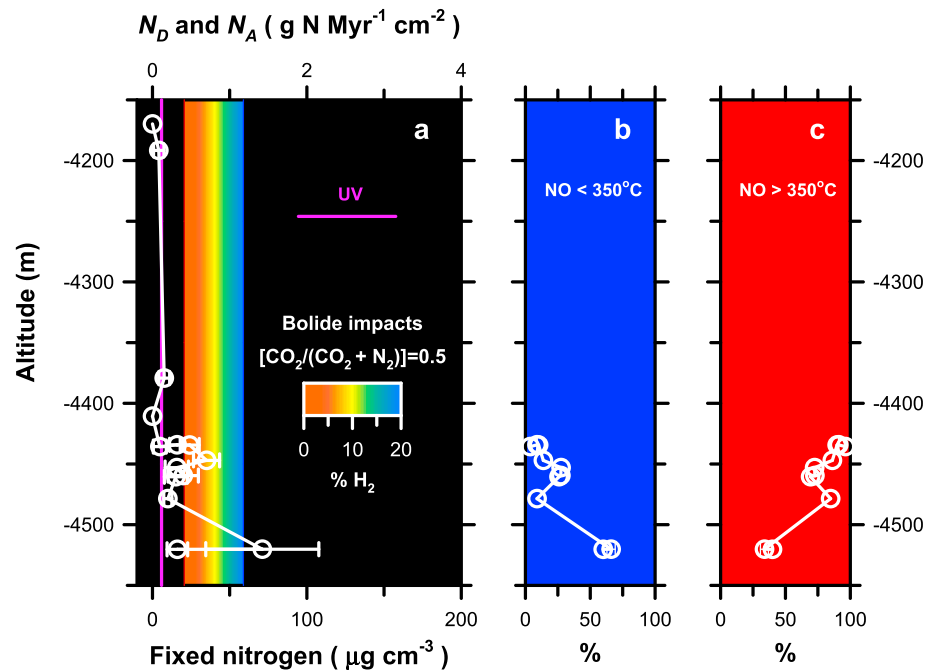
Figure 7. Variation of the amount of nitrogen evolved as NO (a) and its release below (b) and above (c) 350 °C in sedimentary facies measured by SAM along the stratigraphic column from the Yellowknife Bay to the Stimson formations compiled for rocks encountered during the ascent of Curiosity to Aeolis Mons. The upper horizontal axis of panel (a) shows the nitrogen deposition (N_D) and nitrogen accumulation (N_A) rates of nitrogen estimated for Gale crater assuming that all fixed nitrogen deposited over the entire surface of Gale crater was transported into the bottom of the lake using a sediment deposition rate of 20,000 cm/Myr (see section 3.5). The pink line in panel (a) shows the predicted nitrogen deposition for ultraviolet light, whereas the rectangle with the rainbow shows the predicted nitrogen deposition rate by bolide impacts in the absence or presence of H_2 in the atmosphere. The CB sample showed the highest concentration with high variability possibly because it was not well homogenized when supplied to SAM. SAM = Sample Analysis at Mars.

sample was successfully delivered to SAM using a new feed-extended sample transfer technique. The concentration of fixed nitrogen was slightly lower (4 ± 3 μg N/cm^3) than Quela, consistent with a sharp decline of available nitrogen. The last rock sampled was Stoer which again showed no evidence of fixed nitrogen in the form of NO_2^- and NO_3^-.

Figures 7b and 7c and Table S5 show the release of NO below and above 350 °C by the thermal treatment of the rock samples. At the lowest stratigraphic layers, the release of NO below 350 °C dominates, representing about 60–66% of the total NO evolved at −4,519 m; this value drops to ~9% at −4,479 m, then rises to ~27% at −4,455 m, and finally decreases with altitude reaching 0% at −4,428 m (Figure 7b). High values for NO released below 350 °C are associated to the largest numbers of fixed N detected at Gale crater (Figure 7a). The low-temperature release of NO is attributed to NO_2^- and iron-NO_3^-. The opposite behavior was observed for the NO released above 350 °C: Low percentage (34–40%) at −4,519 m, increasing to ~85% at −4,479 m, then declining again ~69% at −4,460 m, and finally rising with altitude reaching 100% at −4,428 m (Figure 7c). High values for NO released above 350 °C are linked to the lowest numbers of fixed N found in the sedimentary rocks at Gale crater (Figure 7a). The high-temperature release of NO is attributed to NO_3^-. The amount of fixed nitrogen found at Gale crater is not as high as previously expected for Mars (Manning et al., 2008), equivalent to the NO_3^- ore deposits found in the subsurface of the hyperarid regions on the Earth (Ericksen, 1983). However, this value falls within the range of abundances reported for the surface of hyperarid environments, such as the Atacama Desert (Sutter et al., 2007) and the Dry Valleys of Antarctica (Michalski et al., 2005).

There are two possible scenarios that could explain the decline of fixed nitrogen of about 2 orders of magnitude along the stratigraphic record in Gale crater: (1) diagenesis and leaching of fixed nitrogen in the sedimentary rocks or (2) change in the rate of nitrogen deposition.

3.4.1. Diagenesis and Leaching of Fixed Nitrogen in the Sedimentary Rocks

Nitrites and/or nitrates present in soils and sedimentary rocks can be leached and transported to lower horizons by the influx of water fluids due to their water solubility. In wet environments they do not accumulate in the surface; however, in hyperarid deserts like the Atacama in Chile, soil nitrates are concentrated below the surface at discrete layers by sporadic rain events. For instance, in Yungay, the driest area in the Atacama with an annual precipitation below 2 mm rain, nitrate is found in a layer between 122 and 146 cm in depth, where the highest concentration is 6.6 mg N/g (Ewing et al., 2006). Below and above this layer the concentration of nitrate sharply decreased. In the historic nitrate deposits of the Atacama that were mined during the early part of the last century, this layer reached concentrations as high as >90 mg N/g for Caliche and > 170 mg N/g for ore grade nitrate (Ericksen, 1983; Semper et al., 1908). In contrast in the wettest part of the Atacama, for example, Copiapó with an annual precipitation of 21 mm, the levels of nitrate are much lower (~83 μg N/g), but interestingly there are two distinctive layers of nitrates centered at 15 and 174 cm, respectively, due to multiple rain events (Ewing et al., 2006). An important feature of these deposits is that all water-insoluble or less soluble salts remain in the upper horizons, whereas the water-soluble salts are leached to lower horizons with nitrate.

The decline of fixed nitrogen found along the stratigraphic record in Gale seems to resemble the leaching of nitrate from the upper stratigraphic layers to the lowest one, as seen in the driest region of the Atacama with three distinct nitrogen layers centered at −4,436, −4,447, and −4,520 m with the lowest exhibiting the highest concentration. No information was available in the literature on the retention and permeability properties of different sedimentary rocks to nitrites and nitrates. Indeed, the sedimentary rocks at Gale crater have been subjected to multiple influxes of ground and underground waters that have altered to various degrees their mineralogy (McLennan et al., 2014; Rampe et al., 2017; Vaniman et al., 2014). However, the evidences against extensive leaching of nitrite and nitrates in the sedimentary rocks at Gale crater are the following: (1) the sedimentary layer retaining NO_2^- and NO_3^- should exhibit a concentration of 10^3 to 10^4 fold greater than the highest value found at Gale crater as found in Atacama; (2) there is a reduced layer of fixed nitrogen (nitrite) below an oxidized layer of nitrate which suggests different deposition conditions; (3) the evolution of NO above 350 °C occurs at different temperatures which indicates the existence of diverse nitrate/oxyclorine salts that were deposited under different geologic settings; (4) there are water-soluble (chlorides, chlorates, perchlorates, nitrites, and nitrates) as well as less soluble (sulfates, sulfides, carbonates, etc) salts in almost all of the layers investigated; and (5) the Sheepbed formation had postdepositional aqueous alteration but with a low water/rock interaction (McLennan et al., 2014; Vaniman et al., 2014). Consequently, this scenario is considered less likely but still possible.

3.4.2. Change in the Rate of Nitrogen Deposition

The abrupt decline of the amount of fixed nitrogen by 1 or 2 orders of magnitude in the stratigraphic record could alternatively imply that the chemistry of the Martian atmosphere drastically changed if it is assumed that energy sources responsible for its formation remained constant during the period when these lacustrine and eolian deposits formed. Our experimental results suggest that a high N fixation rate was possible in the presence of H_2 in the atmosphere. Episodic inputs of H_2 into the atmosphere reaching levels of 10–20% have been proposed as a possible solution for keeping Mars from freezing (Batalha et al., 2015; Ramirez et al., 2014; Wordsworth et al., 2017). The plausible sources of H_2 include (1) serpentinization of minerals containing a high proportion of iron and magnesium, such as olivine ($(Mg,Fe)_2SiO_4$) and pyroxenes ($(Mg,Fe)SiO_3$), which produce H_2-rich fluids (Holm et al., 2015); (2) volcanic emissions of H_2 and reduced carbon from the middle Noachian to the early Amazonian (Batalha et al., 2015; Craddock & Greeley, 2009); (3) impact ablation of meteoritic material impacting the Martian surface (Mimura et al., 2005); (4) iron oxidation by way of UV irradiation of surface waters (Batalha et al., 2015); and (5) photolysis of water (Krasnopolsky & Feldman, 2001). It is generally believed that hydrogen was rapidly lost to space by its decomposition into H by ionospheric processes; however, the hydrogen escape rate is poorly constrained partly because it is not known how water rich early Mars was (Batalha et al., 2015). The *D/H* ratio of water strongly bounded to clays in the Cumberland mudstone analyzed by SAM at Yellowknife Bay provides evidence that hydrogen escaped slowly from the early Martian atmosphere (Mahaffy et al., 2015). In order to maintain a H_2-rich atmosphere for tens to hundreds of thousands of years, it is necessary to remove oxidized compounds from the atmosphere to the surface by wet or dry deposition, and the primordial mantle was considerably more reduced as suggested from the Martian meteorites (Batalha et al., 2015). As H_2 sources were depleted, the rate of

nitrogen fixation by bolide impacts is expected to decline about 10-fold as observed in Figure 7a. Evidence that the early Martian atmosphere was indeed H_2 rich is supported by the speciation of nitrogen in the form of reduced and oxidized layers found in the rock samples investigated by Curiosity. Nitroxyl (HNO) formed in the Martian atmosphere from the reaction of NO with hydrogen atoms arising from the photolysis of water or H_2 (Mancinelli & McKay, 1988) according to reaction (R2):

$$NO + H \rightarrow HNO. \tag{R2}$$

Since HNO is extremely soluble in water, it was efficiently transported by rain onto the Martian surface where it was transformed into $N_xO_x^-$ species that rapidly decayed into NO_3^- and NO_2^- (Mancinelli & Banin, 2003; Summers & Khare, 2007). Both of these species are observed in the lowest stratigraphic layers sampled by Curiosity. As H_2 depleted from the atmosphere, NO reacted with oxygen atoms arising from the photolysis of CO_2, according to reaction (R3):

$$NO + O \rightarrow NO_2. \tag{R3}$$

Dinitrogen oxide (NO_2) reacted with hydroxyl radicals originating from the photolysis of water, according to reaction (R4):

$$NO_2 + OH \rightarrow HNO_3 \rightarrow NO_3^- + H^+. \tag{R4}$$
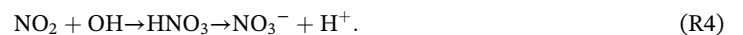
Nitric acid (HNO_3) is extremely soluble in water and would have been efficiently carried to the surface by rain. In this scenario, the N fixation rate by bolide impacts became less efficient and the NO formed converted exclusively to NO_3^-, as observed in the altitudes from −4,427 to −4,192 m (see Figure 7).

The caveat of this scenario is that there are other greenhouse gases that could have kept Mars from freezing (Wordsworth et al., 2017), and possibly the evolution of other reduced atmospheres could lead to a drop in the rate of N fixation and a shift in the type of N species formed, such as CO_2-CH_4-N_2 (Wordsworth et al., 2017) and CO_2-CO-N_2-H_2 (Sholes et al., 2017). Therefore, further laboratory work is required to determine the rate of N fixation by bolide impacts in these atmospheres.

3.5. Nitrogen Deposition and Accumulation Rates Measured by MSL

The nitrogen deposition rate (N_D) for the rocks analyzed by SAM at Gale crater was calculated by multiplying the concentration of fixed nitrogen in the rock ([N] expressed as grams nitrogen per cubic centimeter) by the sediment deposition rate (D is given in centimeters per million years) according to equation (4):

$$N_D = [N] \times D; \tag{4}$$

This implies no losses of fixed nitrogen during the sedimentation process, and consequently N_D represents an upper limit. D is an unknown variable. On Earth D can vary up to 11 orders of magnitude depending on the environmental conditions and geologic time (Sadler, 1981). Kite et al. (2017) have estimated a D value taking into account different alluvial fan deposits on the Martian surface using the occurrence of craters as a fluvial-process chronometer. They derived a D value of <(400–800) cm/Myr. Theoretical modeling for the evolution of Mount Sharp has used D values from 500 to 3,700 cm/Myr, which are consistent with other Mars locations (Borlina et al., 2015). Grotzinger et al. (2014) has used a D value of 100,000 cm/Myr to estimate the length of the lacustrine deposition of the Sheepbed member at Gale crater. We have selected to use an intermediate D value of 20,000 cm/Myr which results in a reasonable fitting of measured values of fixed nitrogen measured for John Klein and Cumberland as can be seen in Figures 3 and 7. N_D varies from 0.3($\pm$0.1) to 1.4($\pm$0.7) g N·Myr^{-1}·cm^{-2} for John Klein and Cumberland, respectively. In contrast, N_F by bolide impacts was calculated to vary from 7×10^{-4} to 2×10^{-3} g N·Myr^{-1}·cm^{-2} at 3250 Myr for the lower and upper and boundaries, respectively (see section 3.2 and Figure 3). These values are significantly smaller by factors of 461 and 711, consecutively. Therefore, it is concluded that atmospheric deposition of nitrogen from bolide impacts directly on the lake surface cannot account for the observed nitrogen concentrations in these sediments. If on the other hand it is considered that nitrogen deposited over the entire surface of Gale crater ($S_G = 1.77 \times 10^4$ km^2) was dissolved, transported, and homogeneously distributed over the entire

surface of the lake (S_L = 30 km^2, Grotzinger et al., 2014) by superficial and ground waters during favorable wet climatic conditions, the nitrogen accumulation rate by bolide impacts (N_A) can be calculated using equation (5).

$$N_A = \frac{N_F \times S_G}{S_L};$$

(5)

N_A increases to 0.4 and 1.2 g N·Myr^{-1}·cm^{-2} for the lower and upper boundaries, correspondingly (see Figures 3 and 7). The upper boundary is, to a first-order approximation, similar to the observed value at Cumberland using a D value of 20,000 cm/Myr. Therefore, our results could imply that the nitrogen found at the Sheepbed unit formed in a H$_2$-rich atmosphere (up to 20%) was deposited on the entire crater's surface, and then it was dissolved, transported, and concentrated into the lake.

The decrease of the nitrogen levels up in the stratigraphic column surveyed by Curiosity (see Figure 7) could indicate a decline of H$_2$ in the atmosphere causing a change in the Martian climate and chemistry of the atmosphere. The predicted N_A values for bolide impacts shown in Figure 7 are the highest possible yields of NO obtained in atmosphere with a CO$_2$/(CO$_2$ + N$_2$) mole ratio of 0.5 with or without H$_2$. Several data points fall below the lower predicted boundary by bolide impacts under this condition. This could indicate that nitrogen fixation by bolide impacts took place in an atmosphere without H$_2$ and a CO$_2$/(CO$_2$ + N$_2$) ratio greater than 0.75 or lower than 0.4 resulting in a reduction in the rate of nitrogen fixation (see section 3.1) as documented for the lack of CO$_3^{2-}$ in the sedimentary rocks found in Gale crater (Bristow et al., 2017). The value obtained from the Cumberland sample is greater than the maximum predicted value for bolide impacts. Possible explanations for this variation include (1) The nitrogen that was dissolved and transported to the lake extended the confines of Gale crater; (2) the sediment deposition rate was not constant along the stratigraphic column investigated by Curiosity; and 3) some degree of diagenesis and leaching of fixed nitrogen took place.

3.6. Comparison With Other Energy Sources

NO was observed in the upper atmosphere by Mars Express (Gagné et al., 2013) and Mars Atmosphere and Volatile EvolutioN Mission (Stiepen et al., 2017). NO and N in the thermosphere through N$_2$ photodissociation in the wavelength from 80 to 100 nm, photoelectron impact dissociation of N$_2$, recombination of N$_2^+$ and NO$^+$, the reaction of N$_2^+$ with O, and the reaction of O$^+$(^{2}P) with N$_2$ (Smith et al., 2014; Yung et al., 1977). Subsequently, N and NO flow toward the lower atmosphere where they are oxidized to NO$_2$, which then reacts with HO$_2$ leading to pernitric acid (HNO$_4$) (Smith et al., 2014). On the Earth, HNO$_4$ is formed in the South Pole's atmosphere by a similar process which is favored at low temperature (Slusher et al., 2002) in a similar temperature regime as to Mars (Smith et al., 2014). This acid is deposited into the Martian surface where it reacts and decomposes into NO$_3^-$ salts. Today this is the most important source of fixed nitrogen to the Martian surface. The N_F by ultraviolet light has been estimated to be 2×10^{-4} g N·Myr^{-1}·cm^{-2} throughout the Amazonian (the last 3000 Myr) when the atmosphere is thought to have been similar to today's cold and hyperarid environment (Smith et al., 2014). The available photochemical models have not considered such high levels of H$_2$ in the Martian atmosphere. Its presence can alter the chemical coupling of N and O in the atmosphere and shift the rate and type N fixed (e.g., HNO, Batalha et al., 2015). However, if we extrapolate this value of N_F to the Hesperian, and if all HNO$_4$ deposited over the entire surface of Gale crater was transported into the lake, N_A would increase to 0.1 g N·Myr^{-1}·cm^{-2}. These values are situated below the lower and upper boundaries set by bolide impacts and consequently are insufficient to account for the N deposition rate derived for Yellowknife Bay (see Figures 3 and 7). The N_A value for UV light corresponds to the lowest levels of N_D depected by SAM (Figure 7). It is estimated that the total mass of N accumulated on the surface of Gale crater during the Amazonian by ultraviolet light alone would be 0.5 g N/cm^2 (Smith et al., 2014), equal to a global deposit of 1.6 cm of sodium nitrate (NaNO$_3$). This is an important amount of nitrate that Curiosity did not detect (J. C. Stern et al., 2015, 2018). Possible explanations to account for its loss in the surface include (1) wind-driven erosion that resulted in partial exhumation of the crater-filling strata (Grotzinger et al., 2015); (2) radiation-induced degradation of nitrates (Zakharov & Nevostruev, 1968) by cosmic rays; and (3) diagenesis and leaching of nitrates into lower sedimentary layers as discussed in section 3.4.

Episodic explosive volcanic eruptions probably occurred in Tharsis and Elysium volcanic provinces, lasting from the Hesperian to the Amazonian (3000 Myr to present) (Xiao et al., 2012). Such eruptions were probably accompanied by copious lightning discharges causing the conversion of N_2 into HCN and/or NO_3^- at high temperatures depending on the nature of the gases emitted by volcanoes (Navarro-González et al., 1998; Segura & Navarro-González, 2001, 2005). The energy flux delivered by volcanic lightning has been calculated during the Hesperian period (Segura & Navarro-González, 2001) considering a global magma production of 5 km^3/year (Xiao et al., 2012). Assuming that all compounds containing fixed N were finally converted into NO_3^-, N_F by volcanic lightning is estimated to be 5×10^{-8} g N·Myr^{-1}·cm^{-2} (Segura & Navarro-González, 2005). If all NO_3^- deposited over the entire surface of Gale crater was transported into the lake, the N_A value would increase to 3×10^{-5} g N·Myr^{-1}·cm^{-2}. These values are below the lower boundary limit set up by bolide impacts by 2 orders of magnitude and therefore are inadequate to account for the NO_3^- deposition rate derived for the Cumberland sample (see Figure 3).

Other energy sources such as cosmic rays, corona and lightning discharges from thunderstorms, and heat from volcanoes had a minor role in N fixation, contributing to a N_F value of $<2 \times 10^{-9}$ g N·Myr^{-1}·cm^{-2} (Segura & Navarro-González, 2005). Recently, it has been argued that coronal mass ejection events from the young Sun, referred to as superflares, generated energetic particles that initiated reactions converting molecular nitrogen, methane, and carbon dioxide into HCN, NO, and N_2O in the early Earth (Airapetian et al., 2016). This is a well-known mechanism where HCN is produced photochemically from N sourced from the ionosphere in a pathway that depends on CH_4 (Tian et al., 2011; Zahnle, 1986). This process was potentially relevant to early Mars, particularly because methane was probably another greenhouse gas present in the atmosphere (Wordsworth et al., 2017), but the type of products fixed and their yields have not been evaluated yet. An additional source of fixed N arises from the exogenous delivery of organics by comets and interplanetary particles to the Martian surface, but its contribution was negligible, for example, $<10^{-9}$ g N·Myr^{-1}·cm^{-2} (Segura & Navarro-González, 2005).

4. Conclusions and Implications

A sharp decline on the amount of fixed nitrogen was found of about 2 orders of magnitude in the rocks sampled by the Curiosity rover during its traverse from the lowest stratigraphic layers encountered on Aeolis Palus to the upper strata of the base of Aeolis Mons. Two possible scenarios were discussed to account for the decline of fixed nitrogen in the stratigraphic record in Gale crater: (1) diagenesis and leaching of fixed nitrogen in the sedimentary rocks or (2) change in the rate of nitrogen deposition.

The decline of fixed nitrogen found in Gale crater seems to resemble the leaching of nitrate from the upper stratigraphic layers to the lowest one, as seen in the driest region of the Atacama with three distinct nitrogen layers centered at −4,436, −4,447, and −4,520 m with the lowest exhibiting the highest concentration. However, the evidences against extensive leaching of nitrite and nitrates in the sedimentary rocks at Gale crater are the following: (1) The concentration of NO_2^- and NO_3^- in the sediments should be higher by 10^3 to 10^4 orders than the highest value observed considering the Atacama nitrate deposits; (2) the existence of a reduced layer of fixed nitrogen (nitrite) below an oxidized layer of nitrate indicates different deposition conditions; (3) the release of NO in the nitrate layer occurs at various temperatures in the different strata investigated indicating the presence of several nitrate/oxychlorine salts and the existence of a variety of sedimentary environments; (4) there are water-soluble as well as less soluble salts in almost all of the layers investigated; and (5) the Sheepbed formation experienced postdepositional aqueous alteration but with a low water/rock interaction. Therefore, diagenesis and leaching of fixed nitrogen in the sedimentary rocks is considered less likely but still possible.

On the other hand, the abrupt decline of the amount of fixed nitrogen could alternatively imply that the chemistry of the Martian atmosphere drastically changed if it is assumed that the energy sources responsible for its formation remained constant during the period when these lacustrine and eolian deposits formed. Our experimental results suggest that a high N fixation rate was possible in the presence of H_2 in the atmosphere. The presence of H_2 from volcanic emissions could have resulted in an enhanced yield in the formation of NO_2^- and NO_3^- by collisions of asteroids into the Martian atmosphere and surface. This enhancement was due to a faster cooling rate of the shock wave freezing NO when its concentration was higher in the heated gas. The impactor flux was used to calculate the nitrogen fixation rate and was found to vary from

7×10^{-4} to 2×10^{-3} g N·Myr^{-1}·cm^{-2} around 3250 Myr ago in the absence or presence of H_2, respectively. In contrast, the nitrogen deposition rate derived from the SAM data at the lowest stratigraphic unit encountered by Curiosity was estimated to vary from 0.3($\pm$0.1) to 1.4($\pm$0.7) g N·Myr^{-1}·cm^{-2} for John Klein and Cumberland, respectively. This value was too high to explain atmospheric NO_2^- and NO_3^- deposition directly on the surface of the lake at Gale crater. It was inferred that fixed nitrogen found at the Sheepbed unit formed in a H_2-rich atmosphere (up to 20%) and was deposited on the entire crater's surface. Upon favorable wet climatic conditions, it was dissolved, transported, and concentrated into the lake by superficial and ground waters. The nitrogen accumulation rate by bolide impacts increases to 0.4 and 1.2 g N·Myr^{-1}·cm^{-2} for the lower and upper boundaries, correspondingly. The value obtained from the Cumberland sample is greater than the maximum predicted value for bolide impacts. Possible explanations for this variation include (1) The nitrogen that was dissolved and transported to the lake extended the confines of Gale crater; (2) the sediment deposition rate was not constant along the stratigraphic column investigated by Curiosity; and (3) some degree of diagenesis and leaching of fixed nitrogen took place.

The nitrogen accumulation rate by ultraviolet light was found to be similar to the lowest nitrogen deposition values derived from the SAM data. Other sources of fixed nitrogen were found to be too small compared to that supplied by bolide impacts to Gale crater.

The caveats of this scenario are that other atmospheric compositions are possible for Mars, such as CO_2-CH_4-N_2 and CO_2-CO-N_2-H_2. Such atmospheres could potentially have an impact on the rate of N fixation and a shift in the type of N species formed as they evolved into CO_2-N_2. Therefore, further laboratory studies are required to determine the rate of N fixation by bolide impacts in these atmospheres.

If the decline of amount of fixed nitrogen found in Gale crater was due to a change in the rate of N deposition, this caused a shortage in the accessibility of fixed nitrogen that could have led to a crisis to microbial life at Gale crater and could have triggered the development of biological nitrogen fixation. A similar nitrogen crisis was inferred for early Earth based on a sharp decline in the NO rate by lightning during the conversion of the atmosphere from mostly CO_2 to primarily N_2 (Navarro-González, McKay, & Nna Mvondo, 2001).

The study of the N and O isotopes present in NO_2^- and NO_3^- from the sediments investigated by Curiosity and other future missions could provide clues on its origin. For instance, nitrate found in the Atacama Desert is known to have been formed in the atmosphere based on mass independent fractionation of O isotopes (Catling et al., 2010). Similar future isotopic analysis of samples returned from Mars may reveal the relative contributions of fixed nitrogen by photochemical or bolides sources in different strata.

References

Airapetian, V. S., Glocer, A., Grono, G., Hébrard, E., & Danchi, W. (2016). Prebiotic chemistry and atmospheric warming of early Earth by an active young Sun. *Nature Geoscience*, *9*(6), 452–455. https://doi.org/10.1038/NGEO2719

Anderson, R. C., Jandura, L., Okon, A. B., Sunshine, D., Roumeliotis, C., Beegle, L. W., et al. (2012). Collecting samples in Gale crater, Mars; an overview of the Mars Science Laboratory sample acquisition, sample processing and handling system. *Space Science Reviews*, *170*(1–4), 57–75. https://doi.org/10.1007/s11214-012-9898-9

Archer, P. D., Franz, H. B., Sutter, B., Arevalo, R. D., Coll, P., Eigenbrode, J. L., et al. (2014). Abundances and implications of volatile-bearing species from evolved gas analysis of the Rocknest aeolian deposit, Gale crater, Mars. *Journal of Geophysical Research: Planets*, *119*, 237–254. https://doi.org/10.1002/2013JE004493

Bale, C. W., Bélisle, E., Chartrand, P., Decterov, S. A., Eriksson, G., Gheribi, A. E., et al. (2016). FactSage thermochemical software and databases, 2010–2016. *Calphad*, *54*, 35–53. https://doi.org/10.1016/j.calphad.2016.05.002

Batalha, N., Domagal-Goldman, S. D., Ramirez, R., & Kasting, J. F. (2015). Testing the early Mars H_2–CO_2 greenhouse hypothesis with a 1-D photochemical model. *Icarus*, *258*, 337–349. https://doi.org/10.1016/j.icarus.2015.06.016

Borlina, C. S., Ehlmann, B. L., & Kite, E. S. (2015). Modeling the thermal and physical evolution of Mount Sharp's sedimentary rocks, Gale crater, Mars: Implications for diagenesis on the MSL Curiosity rover traverse. *Journal of Geophysical Research: Planets*, *120*, 1396–1414. https://doi.org/10.1002/2015JE004799

Bottke, W. F., & Norman, M. D. (2017). The late heavy bombardment. *Annual Review of Earth and Planetary Sciences*, *45*(1), 619–647. https://doi.org/10.1146/annurev-earth-063016-020131

Bristow, T. F., Haberle, R. M., Blake, D. F., Des Marais, D. J., Eigenbrode, J. L., Fairén, A. G., et al. (2017). Low Hesperian pCO$_2$ constrained from in situ mineralogical analysis at Gale crater, Mars. *Proceedings of the National Academy of Sciences of the United States of America*, *114*(9), 2166–2170. https://doi.org/10.1073/pnas.1616649114

Bristow, T. F., Rampe, E. B., Achilles, C. N., Blake, D. F., Chipera, S. J., Craig, P., et al. (2018). Clay mineral diversity and abundance in sedimentary rocks of Gale crater, Mars. *Science Advances*, *4*(6), eaar3330. https://doi.org/10.1126/sciadv.aar3330

Carr, M. H. (1989). Recharge of the early atmosphere of Mars by impact-induced release of CO_2. *Icarus*, *79*(2), 311–327. https://doi.org/10.1016/0019-1035(89)90080-8

Catling, D. C., Claire, M. W., Zahnle, K. J., Quinn, R. C., Clark, B. C., Hecht, M. H., & Kounaves, S. (2010). Atmospheric origins of perchlorate on Mars and in the Atacama. *Journal of Geophysical Research*, *115*, E00E11. https://doi.org/10.1029/2009JE003425

Chameides, W. L. (1979). Effect of variable energy input on nitrogen fixation in instantaneous linear discharges. *Nature*, *277*(5692), 123–124. https://doi.org/10.1038/277123a0

Chameides, W. L., Stedman, D. H., Dickerson, R. R., Rusch, D. W., & Cicerone, R. J. (1977). NO_x production in lightning. *Journal of the Atmospheric Sciences*, *34*(1), 143–149. https://doi.org/10.1175/1520-0469(1977)034<0143:NPIL>2.0.CO;2

Chameides, W. L., & Walker, J. C. (1981). Rates of fixation by lightning of carbon and nitrogen in possible primitive atmospheres. *Origins of Life and Evolution of Biospheres*, *11*(4), 291–302. https://doi.org/10.1007/BF00931483

Craddock, R. A., & Greeley, R. (2009). Minimum estimates of the amount and timing of gases released into the Martian atmosphere from volcanic eruptions. *Icarus*, *204*(2), 512–526. https://doi.org/10.1016/j.icarus.2009.07.026

Do, L., & Raulin, F. (1989). Gas chromatography of Titan's atmosphere. I. Analysis of low-molecular weight hydrocarbons and nitriles with a poraplot Q porous polymer coated open-tubular capillary column. *Journal of Chromatography*, *481*, 45–54. https://doi.org/10.1016/S0021-9673(01)96751-2

Ericksen, G. E. (1983). The Chilean nitrate deposits. *American Scientist*, *71*, 366–374.

Ewing, S. A., Sutter, B., Owen, J., Nishiizumi, K., Sharp, W., Cliff, S. S., Perry, K., et al. (2006). A threshold in soil formation at Earth's arid–hyperarid transition. *Geochimica et Cosmochimica Acta*, *70*(21), 5293–5322. https://doi.org/10.1016/j.gca.2006.08.020

Freissinet, C., Glavin, D. P., Mahaffy, P. R., Miller, K. E., Eigenbrode, J. L., Summons, R. E., et al. (2015). Organic molecules in the Sheepbed Mudstone, Gale crater, Mars. *Journal of Geophysical Research: Planets*, *120*, 495–514. https://doi.org/10.1002/2014JE004737

Gagné, M.‐È., Bertaux, J.‐L., González-Galindo, F., Melo, S. M. L., Montmessin, F., & Strong, K. (2013). New nitric oxide (NO) nightglow measurements with SPICAM/MEx as a tracer of Mars upper atmosphere circulation and comparison with LMD-MGCM model prediction: Evidence for asymmetric hemispheres. *Journal of Geophysical Research: Planets*, *118*, 2172–2179. https://doi.org/10.1002/jgre.20165

Glavin, D. P., Freissinet, C., Miller, K. E., Eigenbrode, J. L., Brunner, A. E., Buch, A., et al. (2013). Evidence for perchlorates and the origin of chlorinated hydrocarbons detected by SAM at the Rocknest Aeolian deposit in Gale crater. *Journal of Geophysical Research: Planets*, *118*, 1955–1973. https://doi.org/10.1002/jgre.20144

Gomes, R., Levison, H. F., Tsiganis, K., & Morbidelli, A. (2005). Origin of the cataclysmic late heavy bombardment period of the terrestrial planets. *Nature*, *435*(7041), 466–469. https://doi.org/10.1038/nature03676

Gough, D. O. (1981). Solar interior structure and luminosity variations. *Solar Physics*, *74*(1), 21–34. https://doi.org/10.1007/BF00151270

Grott, M., Morschhauser, A., Breuer, D., & Hauber, E. (2011). Volcanic outgassing of CO_2 and H_2O on Mars. *Earth and Planetary Science Letters*, *308*(3–4), 391–400. https://doi.org/10.1016/j.epsl.2011.06.014

Grotzinger, J., Gupta, S., Malin, M., Rubin, D., Schieber, J., Siebach, K., et al. (2015). Deposition, exhumation, and paleoclimate of an ancient lake deposit, Gale crater, Mars. *Science*, *350*(6257). https://doi.org/10.1126/science.aac7575

Grotzinger, J. P., Sumner, D. Y., Kah, L., Stack, K., Gupta, S., Edgar, L., et al. (2014). A habitable fluvio-lacustrine environment at Yellowknife Bay, Gale crater, Mars. *Science*, *343*(6169). https://doi.org/10.1126/science.1242777

Hanley, J., Chevrier, V., Berget, D., & Adams, R. (2012). Chlorate salts and solutions on Mars. *Geophysical Research Letters*, *39*, L08201. https://doi.org/10.1029/2012GL051239

Hartmann, W. K., Anguita, J., de la Casa, M. A., Berman, D. C., & Ryan, E. V. (2001). Martian cratering 7: The role of impact gardening. *Icarus*, *149*(1), 37–53. https://doi.org/10.1006/icar.2000.6532

Hartmann, W. K., & Neukum, G. (2001). Cratering chronology and the evolution of Mars. *Space Science Reviews*, *96*(1/4), 165–194. https://doi.org/10.1023/A:1011945222010

Hecht, M. H., Kounaves, S. P., Quinn, R. C., West, S. J., Young, S. M., Ming, D. W., & Smith, P. H. (2009). Detection of perchlorate and the soluble chemistry of Martian soil at the Phoenix Lander site. *Science*, *325*(5936), 64–67. https://doi.org/10.1126/science.1172466

Hogancamp, J. V., Sutter, B., Morris, R. V., Archer, P. D., Ming, D. W., Rampe, E. B., et al. (2018). Chlorate/Fe-bearing phase mixtures as a possible source of oxygen and chlorine detected by the Sample Analysis at Mars (SAM) instrument in Gale crater, Mars. *Journal of Geophysical Research: Planets*, *123*, 2920–2938. https://doi.org/10.1029/2018JE005691

Holm, N. G., Oze, C., Mousis, O., Waite, J. H., & Guilbert-Lepoutre, A. (2015). Serpentinization and the formation of H_2 and CH_4 on celestial bodies (planets, moons, comets). *Astrobiology*, *15*(7), 587–600. https://doi.org/10.1089/ast.2014.1188

Howard, J. B., & Rees, D. C. (1996). Structural basis of biological nitrogen fixation. *Chemical Reviews*, *96*(7), 2965–2982. https://doi.org/10.1021/cr9500545

Hu, R., Kass, D. M., Ehlmann, B. L., & Yung, Y. L. (2015). Tracing the fate of carbon and the atmospheric evolution of Mars. *Nature Communications*, *6*(1), 10003. https://doi.org/10.1038/ncomms10003

Ivanov, B. A. (2001). Mars/moon cratering rate ratio estimates. *Space Science Reviews*, *96*(1/4), 87–104. https://doi.org/10.1023/A:1011941121102

Johnson, R. E., & Liu, M. (1998). Sputtering of the atmosphere of Mars 1. Collitional dissociation of CO_2. *Journal of Geophysical Research*, *103*(E2), 3639–3647. https://doi.org/10.1029/97JE03265

Kahn, R. (1985). The evolution of CO_2 on Mars. *Icarus*, *62*(2), 175–190. https://doi.org/10.1016/0019-1035(85)90116-2

Kite, E. S., Sneed, J., Mayer, D. P., & Wilson, S. A. (2017). Persistent or repeated surface habitability on Mars during the late Hesperian–Amazonian. *Geophysical Research Letters*, *44*, 3991–3999. https://doi.org/10.1002/2017GL072660

Kite, E. S., Williams, J.-P., Lucas, A., & Aharonson, O. (2014). Low palaeopressure of the Martian atmosphere estimated from the size distribution of ancient craters. *Nature Geoscience*, *7*(5), 335–339. https://doi.org/10.1038/ngeo2137

Krasnopolsky, V. A., & Feldman, P. D. (2001). Detection of molecular hydrogen in the atmosphere of Mars. *Science*, *294*(5548), 1914–1917. https://doi.org/10.1126/science.1065569

Kring, D. A., & Cohen, B. A. (2002). Cataclysmic bombardment throughout the inner solar system 3.9–4.0 Ga. *Journal of Geophysical Research*, *107*(E2), 5009. https://doi.org/10.1029/2001JE001529

Levine, J. S., Gregory, G. L., Harvey, G. A., Howell, W. E., Borucki, W. J., & Orville, R. E. (1982). Production of nitric oxide by lightning on Venus. *Geophysical Research Letters*, *9*(8), 893–896. https://doi.org/10.1029/GL009i008p00893

Luo, W., Cang, X., & Howard, A. D. (2016). New Martian valley network volume estimate consistent with ancient ocean and warm and wet climate. *Nature Communications*, *8*, 15766. https://doi.org/10.1038/ncomms15766

Mahaffy, P. R., Webster, C. R., Cabane, M., Conrad, P. G., Coll, P., Atreya, S. K., et al. (2012). The Sample Analysis at Mars investigation and instrument suite. *Space Science Reviews*, *170*(1–4), 401–478. https://doi.org/10.1007/s11214-012-9879-z

Mahaffy, P. R., Webster, C. R., Stern, J. C., Brunner, A. E., Atreya, S. K., Conrad, P. G., et al. (2015). The imprint of atmospheric evolution in the *D/H* of Hesperian clay minerals on Mars. *Science*, *347*(6220), 412–414. https://doi.org/10.1126/science.1260291

Managadze, G. G., Brinckerhoff, W. B., & Chumikov, A. E. (2003). Molecular synthesis in hypervelocity impact plasmas on the primitive Earth and in interstellar clouds. *Geophysical Research Letters*, *30*(5), 1247. https://doi.org/10.1029/2002GL016422

Mancinelli, R. L., & Banin, A. (2003). Where is the nitrogen on Mars? *International Journal of Astrobiology*, *2*(3), 217–225. https://doi.org/10.1017/S1473550403001599

Mancinelli, R. L., & McKay, C. P. (1988). The evolution of nitrogen cycling. *Origins of Life and Evolution of Biospheres*, *18*(4), 311–325. https://doi.org/10.1007/BF01808213

Manion, J. A., Huie, R. E., Levin, R. D., Burgess, Jr., D. R., Orkin, V. L., Tsang, W., et al. (2015). NIST Chemical Kinetics Database, NIST Standard Reference Database 17, Version 7.0 (Web Version), Release 1.6.8, Data version 2015.12, National Institute of Standards and Technology, Gaithersburg, Maryland, 20899-8320. Available from: http://kinetics.nist.gov/ (Accessed 29 January 2017).

Manning, C. V., McKay, C. P., & Zahnle, K. J. (2008). The nitrogen cycle on Mars: Impact decomposition of near-surface nitrates as a source for a nitrogen steady state. *Icarus*, *197*(1), 60–64. https://doi.org/10.1016/j.icarus.2008.04.015

Manning, C. V., Zahnle, K. J., & McKay, C. P. (2009). Impact processing of nitrogen on early Mars. *Icarus*, *199*(2), 273–285. https://doi.org/10.1016/j.icarus.2008.10.015

Markowitz, M. M., & Boryta, D. A. (1965). The differential thermal analysis of perchlorates. VII. Catalytic decompositions of the alkali metal perchlorates by manganese dioxide. *The Journal of Physical Chemistry*, *69*(4), 1114–1123. https://doi.org/10.1021/j100888a005

McKay, C. P., & Borucki, W. J. (1997). Organic synthesis in experimental impact shocks. *Science*, *276*(5311), 390–392. https://doi.org/10.1126/science.276.5311.390

McKay, C. P., & Stoker, C. R. (1989). The early environment and its evolution on Mars: Implication for life. *Reviews of Geophysics*, *27*(2), 189–214. https://doi.org/10.1029/RG027i002p00189

McLennan, S. M., Anderson, R. B., Bell, J. F. III, Bridges, J. C., Calef, F. III, Campbell, J. L., et al. (2014). Elemental geochemistry of sedimentary rocks at Yellowknife Bay, Gale crater, Mars. *Science*, *343*(6169). https://doi.org/10.1126/science.1244734

Melosh, H. J., & Vickery, A. M. (1989). Impact erosion of the primordial atmosphere of Mars. *Nature*, *338*(6215), 487–489. https://doi.org/10.1038/338487a0

Michalski, G., Bockheim, J. G., Kendall, C., & Thiemens, M. (2005). Isotopic composition of Antarctic Dry Valley nitrate: Implications for NO_y sources and cycling in Antarctica. *Geophysical Research Letters*, *32*, L13817. https://doi.org/10.1029/2004GL022121

Mimura, K., Okamoto, M., Nakatsuka, T., Sugitani, K., & Abe, O. (2005). Shock-induced isotope evolution of hydrogen and carbon in meteorites. *Geophysical Research Letters*, *32*, L11201. https://doi.org/10.1029/2005GL023050

Ming, D. W., Archer, P. D. Jr., Glavin, D. P., Eigenbrode, J. L., Franz, H. B., Sutter, B., et al., & MSL Science Team (2014). Volatile and organic compositions of sedimentary rocks in Yellowknife Bay, Gale crater, Mars. *Science*, *343*(6169). https://doi.org/10.1126/science.1245267

Morris, R. V., Vaniman, D. T., Blake, D. F., Gellert, R., Chipera, S. J., Rampe, E. B., et al. (2016). Silicic volcanism on Mars evidenced by tridymite in high-SiO_2 sedimentary rock at Gale crater. *Proceedings of the National Academy of Sciences of the United States of America*, *113*(26), 7071–7076. https://doi.org/10.1073/pnas.1607098113

Navarro K. F. (2014). Síntesis de compuestos nitrogenados por relámpagos en una atmósfera de la Tierra primitiva rica en metano y su impacto en la evolución química. (Bachelor of Science thesis). Retrieved from TESIUNAM. (http://132.248.9.195/ptd2014/mayo/0713318/Index.html). Ciudad Universitaria, Ciudad de México, Mexico: Universidad Nacional Autónoma de México.

Navarro-González, R., McKay, C. P., & Nna Mvondo, D. (2001). A possible nitrogen crisis for Archaean life due to reduced nitrogen fixation by lightning. *Nature*, *412*(6842), 61–64. https://doi.org/10.1038/35083537

Navarro-González, R., Molina, M. J., & Molina, L. T. (1998). Nitrogen fixation by volcanic lightning in the early Earth. *Geophysical Research Letters*, *25*(16), 3123–3126. https://doi.org/10.1029/98GL02423

Navarro-González, R., Stern, J., Sutter, B., Archer, D., McAdam, A., Franz, H. B., et al. (2013). Possible detection of nitrates on Mars by the Sample Analysis at Mars (SAM) instrument. *LPI Contrib.*, *1719*, 2648.

Navarro-González, R., Villagrán-Muniz, M., Sobral, H., Molina, L. T., & Molina, M. J. (2001). The physical mechanism of nitric oxide formation in simulated lightning. *Geophysical Research Letters*, *28*(20), 3867–3870. https://doi.org/10.1029/2001GL013170

Nna Mvondo, D., Navarro-González, R., McKay, C.P., Coll, P. &. Raulin, F. (2001). Production of nitrogen oxides by lightning and coronae discharges in simulated early Earth, Venus and Mars environments. *Advances in Space Research 27*(2), 217–223. https://doi.org/10.1016/S0273-1177(01)00050-3

Panarella, E. (1974). Theory of laser-induced gas ionization. *Foundations of Physics*, *4*(2), 227–259. https://doi.org/10.1007/BF00712689

Pham, L. B. S., & Karatekin, Ö. (2016). Scenarios of atmospheric mass evolution on Mars influenced by asteroid and comet impacts since the late Noachian. *Planetary and Space Science*, *125*, 1–11. https://doi.org/10.1016/j.pss.2015.09.022

Pollack, J. B., Kasting, J. F., Richardson, S. M., & Poliakoff, K. (1987). The case for a wet, warm climate on early Mars. *Icarus*, *71*(2), 203–224. https://doi.org/10.1016/0019-1035(87)90147-3

Postgate, J. (1996). *Nitrogen fixation*. Cambridge, UK: Cambridge University Press.

Rahman, M., & Cooray, V. (2008). A study of NO_X production in air heated by laser discharges: Effect of energy, wavelength, multiple discharges and pressure. *Optics and Laser Technology*, *40*(1), 208–214. https://doi.org/10.1016/j.optlastec.2007.01.007

Ramirez, R. M., Kopparapu, R., Zugger, M. E., Robinson, T. D., Freedman, R., & Kasting, J. F. (2014). Warming early Mars with CO_2 and H_2. *Nature Geoscience*, *7*(1), 59–63. https://doi.org/10.1038/ngeo2000

Rampe, E. B., Ming, D. W., Blake, D. F., Bristow, T. F., Chipera, S. J., Grotzingerd, J. P., et al. (2017). Mineralogy of an ancient lacustrine mudstone succession from the Murray formation, Gale crater, Mars. *Earth and Planetary Science Letters*, *471*, 172–185. https://doi.org/10.1016/j.epsl.2017.04.021

Sadler, P. M. (1981). Sediment accumulation rates and the completeness of stratigraphic sections. *The Journal of Geology*, *89*(5), 569–584. https://doi.org/10.1086/628623

Sagan, C. (1977). Reducing greenhouses and temperature history of Earth and Mars. *Nature*, *269*(5625), 224–226. https://doi.org/10.1038/269224a0

Samarkin, V. A., Madigan, M. T., Bowles, M. W., Casciotti, K. L., Priscu, J. C., McKay, C. P., & Joye, S. B. (2010). Abiotic nitrous oxide emission from the hypersaline Don Juan pond in Antarctica. *Nature Geoscience*, *3*(5), 341–344. https://doi.org/10.1038/NGEO847

Sasoh, A. (2016). Laser focusing. In O. Igra & F. Seiler (Eds.), *Experimental methods of shock wave research*, *Shock Wave Science and Technology Reference Library 9* (pp. 99–108). Basel, Switzerland: Springer International Publishing.

Scattergood, T. W., McKay, C. P., Borucki, W. J., Giver, L. P., van Ghyseghem, H., Parris, J. E., & Miller, S. L. (1989). Production of organic compounds in plasmas: A comparison among electric sparks, laser-induced plasmas, and UV light. *Icarus*, *81*(2), 413–428. https://doi.org/10.1016/0019-1035(89)90061-4

Segura, A., & Navarro-González, R. (2001). Experimental simulation of early Martian volcanic lightning. *Advances in Space Research*, *27*(2), 201–206. https://doi.org/10.1016/S0273-1177(01)00048-5

Segura, A., & Navarro-González, R. (2005). Nitrogen fixation on early Mars by volcanic lightning and other sources. *Geophysical Research Letters*, *32*, L05203. https://doi.org/10.1029/2004GL021910

Semper, E., Michels, G.-M. J., & Ghigliotto-Salas, O. (1908). La Industria del Salitre en Chile. *Metalurjia i Sustancias Salinas*, *52*, 1–418.

Sholes, S. F., Smith, M. L., Claire, M. W., Zahnle, K. J., & Catling, D. C. (2017). Anoxic atmospheres on early Mars driven by volcanism: Implications for past environments and life. *Icarus*, *290*, 46–62. https://doi.org/10.1016/j.icarus.2017.02.022

Slusher, D. L., Huey, L. G., Tanner, D. J., Chen, G., Davis, D. D., Buhr, M., et al. (2002). Measurements of pernitric acid at the South Pole during ISCAT 2000. *Geophysical Research Letters*, *29*(21), 2011. https://doi.org/10.1029/2002GL015703

Smith, M. L., Claire, M. W., Catling, D. C., & Zahnle, K. J. (2014). The formation of sulfate, nitrate and perchlorate salts in the Martian atmosphere. *Icarus*, *231*, 51–64. https://doi.org/10.1016/j.icarus.2013.11.031

Sobral, H., Villagrán-Muniz, M., Navarro-González, R., & Raga, A. C. (2000). Temporal evolution of the shock wave and hot core air in laser induced plasma. *Applied Physics Letters*, *77*(20), 3158–3160. https://doi.org/10.1063/1.1324986

Stern, J. C., Sutter, B., Archer, P. D., Eigenbrode, J. L., McAdam, A. C., Franz, H. B., et al. (2018). Major volatiles evolved from eolian materials in Gale crater. *Geophysical Research Letters*, *45*(19), 10,240–10,248. https://doi.org/10.1029/2018GL079059

Stern, J. C., Sutter, B., Freissinet, C., Navarro-González, R., McKay, C. P., Archer, P. D. Jr., et al. (2015). Evidence for indigenous nitrogen in sedimentary and aeolian deposits from the Curiosity rover investigations at Gale crater, Mars. *Proceedings of the National Academy of Sciences of the United States of America*, *112*(14), 4245–4250. https://doi.org/10.1073/pnas.1420932112

Stern, J. C., Sutter, B., Jackson, W. A., Navarro-González, R., McKay, C. P., Ming, D. W., et al. (2017). The nitrate/(per) chlorate relationship on Mars. *Geophysical Research Letters*, *44*, 2643–2651. https://doi.org/10.1002/2016GL072199

Stern, K. H. (1972). High temperature properties and decomposition of inorganic salts. Part 3. Nitrates and nitrites. *Journal of Physical and Chemical Reference Data*, *1*(3), 747–772. https://doi.org/10.1063/1.32531041

Stiepen, A., Jain, S. K., Schneider, N. M., Deighan, J. I., González-Galindo, F., Gérard, J.-C., et al. (2017). Nitric oxide nightglow and Martian mesospheric circulation from MAVEN/IUVS observations and LMD-MGCM predictions. *Journal of Geophysical Research: Space Physics*, *122*, 5782–5797. https://doi.org/10.1002/2016JA023523

Stribling, R., & Miller, S. L. (1987). Energy yields for hydrogen cyanide and formaldehyde syntheses: The HCN and amino acid concentrations in the primitive ocean. *Origins of Life and Evolution of Biospheres*, *17*(3–4), 261–273. https://doi.org/10.1007/BF02386466

Strom, R. G., Malhotra, R., Ito, T., Yoshida, F., & Kring, D. A. (2005). The origin of planetary impactors in the inner solar system. *Science*, *309*(5742), 1847–1850. https://doi.org/10.1126/science.1113544

Summers, D. P., & Khare, B. (2007). Nitrogen fixation on early Mars and other terrestrial planets: Experimental demonstration of abiotic fixation reactions to nitrite and nitrate. *Astrobiology*, *7*(2), 333–341. https://doi.org/10.1089/ast.2006.0032

Sutter, B., Dalton, J. B., Ewing, S. A., Amundson, R., & McKay, C. P. (2007). Terrestrial analogs for interpretation of infrared spectra from the Martian surface and subsurface: Sulfate, nitrate, carbonate, and phyllosilicate-bearing Atacama Desert soils. *Journal of Geophysical Research*, *112*, G04S10. https://doi.org/10.1029/2006JG000313

Sutter, B., McAdam, A. C., Mahaffy, P. R., Ming, D. W., Edgett, K. S., Rampe, E. B., et al. (2017). Evolved gas analyses of sedimentary rocks and eolian sediment in Gale crater, Mars: Results of the Curiosity rover's Sample Analysis at Mars (SAM) instrument from Yellowknife Bay to the Namib Dune. *Journal of Geophysical Research: Planets*, *122*, 2574–2609. https://doi.org/10.1002/2016JE005225

Tian, F., Kasting, J. F., & Zahnle, K. (2011). Revisiting HCN formation in Earth's early atmosphere. *Earth and Planetary Science Letters*, *308*(3-4), 417–423. https://doi.org/10.1016/j.epsl.2011.06.011

Tomkinson, T., Lee, M. R., Mark, D. F., & Smith, C. L. (2013). Sequestration of Martian CO_2 by mineral carbonation. *Nature Communications*, *4*(1), 2662. https://doi.org/10.1038/ncomms3662

Vaniman, D. T., Bish, D. L., Ming, D. W., Bristow, T. F., Morris, R. V., Blake, D. F., et al. (2014). Mineralogy of a mudstone at Yellowknife Bay, Gale crater, Mars. *Science*, *343*(6169). https://doi.org/10.1126/science.1243480

von Paris, P., Grenfell, J. L., Rauer, H., & Stock, J. W. (2013). N_2-associated surface warming on early Mars. *Planetary and Space Science*, *82-83*, 149–154. https://doi.org/10.1016/j.pss.2013.04.009

Wordsworth, R., Kalugina, Y., Lokshtanov, S., Vigasin, A., Ehlmann, B., Head, J., et al. (2017). Transient reducing greenhouse warming on early Mars. *Geophysical Research Letters*, *44*, 665–671. https://doi.org/10.1002/2016GL071766

Wordsworth, R., & Pierrehumbert, R. (2013). Hydrogen-nitrogen greenhouse warming in Earth's early atmosphere. *Science*, *339*(6115), 64–67. https://doi.org/10.1126/science.1225759

Wordsworth, R. D. (2016). The climate of early Mars. *Annual Review of Earth and Planetary Sciences*, *44*(1), 381–408. https://doi.org/10.1146/annurev-earth-060115-012355

Xiao, L., Huang, J., Christensen, P. R., Greeley, R., Williams, D. A., Zhao, J., & He, Q. (2012). Ancient volcanism and its implication for thermal evolution of Mars. *Earth and Planetary Science Letters*, *323-324*, 9–18. https://doi.org/10.1016/j.epsl.2012.01.027

Yeung, L. Y., Li, S., Kohl, I. E., Haslun, J. A., Ostrom, N. E., Hu, H., et al. (2017). Extreme enrichment in atmospheric $^{15}N^{15}N$. *Science Advances*, *3*(11), eaao6741. https://doi.org/10.1126/sciadv.aao6741

Yung, Y. J., Strobel, D., Kong, T. Y., & McElroy, M. B. (1977). Photochemistry of nitrogen in the Martian atmosphere. *Icarus*, *30*(1), 26–41. https://doi.org/10.1016/0019-1035(77)90118-X

Zahnle, K. J. (1986). Photochemistry of methane and the formation of hydrocyanic acid (HCN) in the Earth's early atmosphere. *Journal of Geophysical Research*, *91*(D2), 2819–2834. https://doi.org/10.1029/JD091iD02p02819

Zakharov, Y. A., & Nevostruev, V. A. (1968). Radiolysis of solid inorganic salts with oxygen-containing anions. *Russian Chemical Reviews*, *37*(1), 61–73. https://doi.org/10.1070/RC1968v037n01ABEH001608

Zel'dovitch, Y. B., & Raizer, Y. O. (1966). *Physics of shock waves and high-temperature hydrodynamic phenomena*. New York, NY: Academic Press.